Links between acceleration, melting, and supraglacial lake drainage of the western Greenland Ice Sheet

M. J. Hoffman[1,2,3], G. A. Catania[4,5], T. A. Neumann[1], L. C. Andrews[5], J. A. Rumrill[6]

[1]Cryospheric Sciences Branch, NASA Goddard Space Flight Center, Greenbelt, Maryland, 20771, USA

[2]Joint Center for Earth Systems Technology, University of Maryland, Baltimore County, Baltimore, Maryland, 21228, USA

[3]now at Fluid Dynamics Group, Los Alamos National Laboratory, Los Alamos, New Mexico, 87545, USA

[4]Institute for Geophysics, University of Texas, Austin, Texas, 78759, USA

[5]Department of Geological Sciences, University of Texas, Austin, Texas, 78712, USA

Abstract. The impact of increasing summer melt on the dynamics and stability of the Greenland Ice Sheet is not fully understood. Mounting evidence suggests seasonal evolution of subglacial drainage mitigates or counteracts the ability of surface runoff to increase basal sliding. Here, we compare subdaily ice velocity and uplift derived from nine Global Positioning System stations in the upper ablation zone in west Greenland to surface melt and supraglacial lake drainage during summer 2007. Starting around day 173, we observe speedups of 6-41% above spring velocity lasting ∼40 days accompanied by sustained surface uplift at most stations, followed by a late summer slowdown. After initial speedup, we see a spatially uniform velocity response across the ablation zone and strong diurnal velocity variations during periods of melting. Most lake drainages were undetectable in the velocity record, and those that were detected only perturbed velocities for ∼1 day, suggesting preexisting drainage systems could efficiently drain large volumes of water. The dynamic response to melt forcing appears to 1) be driven by changes in subglacial storage of water that is delivered in diurnal and episodic pulses, and 2) decrease over the course of the summer, presumably as the subglacial drainage system evolves to greater efficiency. The relationship be-

[6]Earth Science Department, Southern
Connecticut State University, New Haven,
Connecticut, 06515, USA

tween hydrology and ice dynamics observed is similar to that observed on mountain glaciers, suggesting that seasonally large water pressures under the ice sheet largely compensate for the greater ice thickness considered here. Thus, increases in summer melting may not guarantee faster seasonal ice flow.

1. INTRODUCTION

Basal lubrication by surface meltwater penetrating the Greenland Ice Sheet generates summer speedups of 50-200% for the regions of the ablation zone experiencing sheet flow [*Zwally et al.*, 2002; *Joughin et al.*, 2008; *van de Wal et al.*, 2008; *Shepherd et al.*, 2009; *Bartholomew et al.*, 2010; *Sundal et al.*, 2011; *Palmer et al.*, 2011]. This seasonal acceleration has led to uncertainty in the dynamic sensitivity of the Greenland Ice Sheet mass balance to increased atmospheric temperatures [*Bamber et al.*, 2007; *Shepherd et al.*, 2009]. If surface melting translates directly to increased sliding, rising temperatures could generate a positive feedback to mass loss as faster flow causes the ice sheet to lower into warmer elevations [*Zwally et al.*, 2002; *Parizek and Alley*, 2004]. On the other hand, if the subglacial hydrologic system of the ice sheet adapts to variable meltwater input, as observed on mountain glaciers [e.g. *Iken and Bindschadler*, 1986; *Mair et al.*, 2002a; *Bartholomaus et al.*, 2008], increased melt could generate a limited, or even decelerating, effect on seasonally-averaged sliding and long-term dynamic response to warming climate [*Truffer et al.*, 2005; *van de Wal et al.*, 2008; *Sundal et al.*, 2011; *Schoof*, 2010].

Recent observations have presented mounting evidence for a seasonal and spatial evolution of the subglacial hydrologic system of the Greenland Ice Sheet that mitigates the impact of meltwater lubrication. The relationship between melt and velocity varies substantially over the course of the melt season [*Bartholomew et al.*, 2010; *Sundal et al.*, 2011] and in space, both longitudinally and laterally [*Bartholomew et al.*, 2010; *Palmer et al.*, 2011], while variations in the quantity and composition of proglacial discharge indicate a seasonal increase in the efficiency of the subglacial drainage [*Bartholomew et al.*, 2011].

Additionally, evidence for evolution of the subglacial hydrologic system has been observed in fast-moving, marine-terminating outlet glaciers in Greenland [*Howat et al.*, 2010; *Andersen et al.*, 2010], though the effect on outlet glaciers is generally small relative to other dynamic processes [*Joughin et al.*, 2008; *Andersen et al.*, 2011]. These recent studies build on previous observations that revealed an ambiguous relationship between seasonal melt and velocity at decadal scales [*van de Wal et al.*, 2008], the existence of diurnal variations in velocity during summer [*Shepherd et al.*, 2009], and the existence of persistent englacial pathways capable of consistently routing large quantities of water to the bed [*Das et al.*, 2008; *Catania and Neumann*, 2010].

Despite these advances, questions remain regarding the relationship between surface hydrology and dynamics of the Greenland Ice Sheet. Recent observations have been focused on a small area near Kangerlussuaq in southwest Greenland [*van de Wal et al.*, 2008; *Shepherd et al.*, 2009; *Bartholomew et al.*, 2010; *Sundal et al.*, 2011; *Palmer et al.*, 2011; *Bartholomew et al.*, 2011], and their applicability to other locations on the ice sheet experiencing sheet flow remains untested. Furthermore, modeling studies suggest the importance of subdaily links between surface hydrology and velocity [*Schoof*, 2010; *Pimentel and Flowers*, 2010], which is beyond the temporal resolution of most existing studies. Additionally, the role of supraglacial lake drainage [*Box and Ski*, 2007; *Das et al.*, 2008] and longitudinal flow coupling [*Price et al.*, 2008] in seasonal velocity variations remains unclear. Finally, due to the lack of subglacial observations on ice sheets, the basal hydrology of well-studied mountain glaciers has been routinely suggested as an analog for that of the ice sheet [*Truffer et al.*, 2005; *van de Wal et al.*, 2008; *Bartholomaus et al.*, 2008; *Shepherd et al.*, 2009; *Bartholomew et al.*, 2010, 2011; *Sundal et al.*, 2011]. However,

the thickness of the ice sheet in many places (∼1000 m) is up to an order of magnitude greater than that of many well-studied mountain glaciers, which would cause the creep closure of low-pressure subglacial channels within hours (as opposed to days or weeks for thinner glaciers) [*Nye*, 1953; *Bartholomaus et al.*, 2008; *Catania and Neumann*, 2010] and could impact the formation and persistence of subglacial channels. Other differences on the ice sheet are longer distances to the ice terminus and decreased lateral drag. The importance of these differences in using mountain glaciers as analogs for the ice sheet remains largely unresolved.

Here we present Global Positioning System (GPS) data from a transect near Swiss Camp (69.57°N 49.33°W) in west Greenland (Figure 1) from summer 2007. These data record three distinct modes of variability in ice sheet surface velocity; seasonal, diurnal and episodic events. We compare these observations to melt estimated with a positive degree day (PDD) model and an inventory of lake drainage. We use this set of observations to assess the nature of the subglacial hydrologic system, its seasonal evolution, and the relative importance of meltwater, lake drainages, and longitudinal flow coupling to the ice dynamics in the region.

2. DATA AND METHODS

We compare melt intensity variations and episodic lake drainage events to ice velocity measured at nine GPS stations across a study area spanning ∼50 km of the western Greenland Ice Sheet (Figure 1, Table 1). For convenience, we define downglacier (GPS stations 107, 207, 307), midglacier (GPS stations 407, 507, Wild1), and upglacier (GPS stations 607, 707, 807) regions. During the 1980s, the equilibrium line altitude in this area was between 1000 and 1250 m a.s.l. [*Ahlstrøm*, 2007], which encompasses our midglacier

region, although more recent observations [*Zwally et al.*, 2002] and mass balance modeling [*Mernild et al.*, 2008] suggest that the equilibrium zone may extend up to 1400 m a.s.l., approximately the elevation of our highest station (807). Snowcover extent and the filling and draining of supraglacial lakes was determined from available cloud-free Landsat ETM imagery at approximately biweekly time intervals between early June and late August during summer 2007 (days 157, 173, 189, 205, and 234). The end of summer snowline in the area occurred at about 1300 m a.s.l. in 2007. All times are reported in Coordinated Universal Time (UTC), which is two hours ahead of local time during summer. Solar noon in the area occurs at approximately 15:20 UTC during summer.

2.1. Temperature and Melt

We estimate surface melting using mean hourly temperature data from two weather stations (JAR1 at 960 m a.s.l. and Swiss Camp at 1150 m a.s.l., Figure 1) that are part of the GC-Net weather station array [*Steffen and Box*, 2001]. Temperature was measured with a Vaisala CS-500 probe and has an accuracy of 0.1 °C [*Steffen and Box*, 2001]. Because spatial variation in temperature over tens of km is primarily controlled by elevation, we consider the JAR1 weather station to be representative of the downglacier region and the Swiss Camp weather station to be representative of the midglacier region. For the upglacier region, we extrapolated temperature to the average elevation of the upglacier stations (1330 m.a.s.l) using the hourly lapse rate between JAR1 and Swiss Camp.

In Greenland, PDD are highly correlated with melt [*Braithwaite and Olesen*, 1987; *Braithwaite*, 1995], and degree day modeling can provide estimates of melt that are comparable to more complex energy balance modeling [*van de Wal*, 1996]. Therefore, we

estimate water equivalent (w.e.) melt using a degree-day model applied for each region:

$$M = \beta_{snow,ice} PDD \tag{1}$$

in which M is daily melt in mm w.e. and PDD is the peak positive hourly temperature reached per day. β is the degree-day factor and is set to 3 mm w.e. d^{-1} $^{\circ}C^{-1}$ for snow and 14 mm w.e. d^{-1} $^{\circ}C^{-1}$ for ice, following the parameterization of *Fausto et al.* [2009]. Within each of our three regions, we used the six Landsat images to classify the glacier surface as covered by snow, patchy snow, or ice. For the time periods classified as patchy snow, we linearly interpolated β between snow and ice values. The upglacier region remained about half snow covered on day 205 (9 August), and so we interpolated β between a snow value on day 189 (24 July) and an area-weighted value of 8 mm w.e. d^{-1} $^{\circ}C^{-1}$ on day 234 (22 August), at which time new snow covered the entire upglacier region. The low temporal resolution of snowline retreat introduces uncertainty in the degree-day factor, but we assume that we have captured the seasonal evolution of albedo and melt rate. Because we do not have ablation measurements with which to calibrate the melt model, we consider the output to simply represent seasonal variations in relative daily melt intensity.

2.2. Supraglacial Lake Drainage

Manual inspection of the six Landsat images was used to identify the location, size, and approximate timing of the filling and draining of supraglacial lakes. Lakes appearing between sequential images were counted as lakes that filled in the interval between image acquisition, while lakes that disappeared between sequential images were counted as lakes that drained. We counted the number of lakes draining and filling between each of the six Landsat images within a distance of 5 km of each GPS station (Figure 1). The 5 km

distance was chosen based on the typical distances between supraglacial lakes and moulins in our field area [*Catania et al.*, 2008], as well as predictions of the flow coupling length scale in the region [*Price et al.*, 2008]. Radar profiles in a 150 km^2 region encompassing our GPS stations identified 32 probable moulins [*Catania et al.*, 2008; *Catania and Neumann*, 2010], suggesting that, on average, surface water must travel about 1.5 km before being intercepted by a moulin. We assume that no lakes drained prior to our first Landsat image on day 157 (June 6).

Our satellite imagery indicates where and over what time period surface lakes drain, but not the mechanism of draining, nor the volume of water released. We use lake diameter as a proxy for volume, but acknowledge that this introduces significant uncertainty. Lakes can drain either over the ice surface through breaching, or down through the ice via moulin formation or re-activation [*Das et al.*, 2008]. Prior work in the area suggests that there are relatively few, if any, moulins inland of the equilibrium line, and that a few moulins may drain the equivalent of dozens of lakes before becoming inactive [*Catania and Neumann*, 2010].

2.3. Ice Velocity

We deployed nine GPS receivers (Trimble NetR7 with Trimble Zephyr Geodetic antennas) sampling at 15 s on the ice sheet surface (Figure 1) in May 2007. GPS antennas were mounted on plywood platforms ∼1.5 m above the snow/ice surface, supported by three steel poles inserted 2 m into the glacier surface following the method of *Anderson et al.* [2004]. Each station was powered by solar panels and 12V batteries to provide continuous records of position through the summer, although data gaps occurred at some stations due to loss of power (burial of solar panels by snow) or melt-out of the GPS antenna. The

receivers were arranged roughly along a flow line from the upper estimate of the equilibrium line downstream 40 km into the ablation zone. Additional stations were placed up to a few kilometers off-axis to observe variations in transverse ice velocity (Figure 1). This arrangement was designed to detect regional variations in ice velocity along the flow line.

Kinematic GPS positions were determined by carrier-phase differential processing relative to bedrock-mounted reference stations using Track v.1.22 software [*Chen*, 1998] using final International GNSS Service satellite orbits. Generally, the KAGA reference station was used with baselines of 30 to 62 km (Figure 1) but when unavailable, the KELY (290 km baseline) or KULU (720 km baseline) reference stations were used instead. The data were processed using the maximum temporal resolution of available reference station data, which was 15 s at KAGA prior to day 214 (2 August) of 2007, and 30 s at KELY and KULU and at KAGA after day 217 of 2007. Though typical velocity in this area is $\sim$100 m a^{-1} [*Zwally et al.*, 2002], kinematic site motion was constrained on an epoch-by-epoch basis to an equivalent of 2000 m a^{-1} to allow for short duration velocity increases that may be associated with supraglacial lake drainage [e.g. *Das et al.*, 2008]. Tropospheric delays were modeled in Track with a constraint that allows for variations up to 35 cm d^{-1}.

After processing, positions were filtered with a 6-hr moving average to suppress spurious signals due to GPS uncertainties and decimated to create a position time-series with 15-min temporal resolution. Data for stations 107-507 are unusable after day 213 (1 August) due to high ablation rates causing antennas to tip, and all stations suffer from extended data gaps between days 213 and 224 due to base station outages. Sidereally repeating noise

due to multipath errors produced deviations from mean horizontal motion as much as 2.5 cm over tens of minutes. Modified sidereal filtering [*Choi et al.*, 2004] eliminates most of these signals, but the sidereal noise pattern occasionally changes abruptly, presumably due to the multipath environment changing due to snowfall, ablation, or wind redistribution of snow, making such a correction inappropriate for our dataset. We identify a period of constant background motion at each station at the beginning of summer prior to day 158 at Station 107 and lasting longer at stations farther inland. By assuming steady ice movement during the background period prior to day 158 (19-25 days depending on station), we estimate uncertainty of the moving average filtered position time-series to be 4 mm horizontally and 20 mm vertically.

Using the filtered 15-minute position time-series, we calculated three horizontal velocity products to emphasize motion at seasonal, diurnal, and event time scales. We calculated a 24-hr mean velocity dataset using a centered 24-hr time window applied at each data point in the 15-minute position time series. The resulting velocity time-series has data points at 15-minute intervals and with time windows that overlap. The advantage to this approach is that it avoids aliasing that may occur from using non-overlapping, discrete time intervals. The 24-hr mean velocity calculation largely eliminates diurnal velocity variations while retaining low frequency seasonal velocity variations and high frequency (<24 hr) events. The 24-hr mean velocity calculation reduces the amplitude of high frequency events, but does not cause a phase shift. The second velocity data product is 6-hr mean velocity calculated in the same fashion, which emphasizes diurnal variations in velocity. Finally, for large amplitude events with high signal-to-noise ratio, we calculated 2-hr mean velocity. The 24-hr mean velocity data have an uncertainty of $\sim$4 m a^{-1} (3-6%

of the background velocity), the 6-hr mean velocity data have an uncertainty of $\sim$10 m a^{-1} (8-15% of the background velocity), and the 2-hr mean velocity data have an uncertainty of $\sim$15 m a^{-1}.

2.4. Strain rates

We calculated strain rates in order to assess the contribution of vertical strain to observed vertical surface motion. Daily longitudinal (along-flow) and lateral (across-flow) strain rates from the GPS data were calculated using

$$\dot{\epsilon} = \frac{1}{l_o}\frac{\Delta l}{\Delta t} \tag{2}$$

where Δl is the change in baseline distance between stations along a flow line, Δt is 24 hours and l_o is the initial distance between stations (Table 2) [*Rumrill*, 2009].

We approximated vertical strain rate using the continuity equation and assuming ice is incompressible:

$$\dot{\epsilon}_{zz} = -(\dot{\epsilon}_{xx} + \dot{\epsilon}_{yy}) \tag{3}$$

where the subscripts x, y and z represent the longitudinal, lateral and vertical strain rates, respectively.

We estimated a time-series of vertical displacement, D_ϵ, due to vertical strain following *Anderson et al.* [2004] and *Howat et al.* [2008]

$$D_\epsilon = -H\Delta t\dot{\epsilon}_{zz} \tag{4}$$

where H is ice thickness.

2.5. Bed Separation

Vertical ice motion, which is measured by the GPS receivers, can be separated into three components: the vertical component of mean bed-parallel motion, vertical strain, and vertical motion of basal ice relative to the bed (bed separation/cavity formation plus dilation of subglacial sediments, if present) [*Anderson et al.*, 2004]. Bed separation is the component most directly related to basal sliding, and is our focus here. To separate these components from the measured vertical motion at the surface, w_s, we followed the method first described by *Hooke et al.* [1989] and now in common use [e.g. *Mair et al.*, 2002a, b; *Anderson et al.*, 2004; *Sugiyama and Gudmundsson*, 2004; *Harper et al.*, 2007; *Howat et al.*, 2008]:

$$w_s = u_b \tan\alpha + \dot{\epsilon}_{zz} H + \dot{c} \tag{5}$$

where u_b is the horizontal component of the sliding velocity, α is the bed slope, and $\dot{c}$ is the rate of cavity opening, including the effects of till dilation.

Because the proper length-scale at which to measure α is not clear [*Mair et al.*, 2002b] and radar-echo sounding indicates bed slope in the region varies over different length-scales [*Catania et al.*, 2008], we calculated the vertical component of bed parallel motion as a residual during the background period of steady motion (prior to day 158), over which we assume that the components of vertical motion due to bed-parallel motion and vertical strain are each constant and the rate of cavity opening is zero:

$$u_{b,bg} \tan\alpha = w_{s,bg} - \dot{\epsilon}_{zz_{s,bg}} H \tag{6}$$

where the subscripts $_b$ and $_s$ denote values at the bed and surface, respectively, and $_{bg}$ denotes the background time period. The uncertainty in the vertical component of mean bed-parallel motion is about 0.8 mm d^{-1} (see the Appendix). The total horizontal ice motion during the summer is <50 m, and the ice thickness (>500 m) is such that bed features with wavelengths less than the ice thickness are not expressed at the ice surface [*Gudmundsson*, 2003]. As a consequence, we assume that α is constant over the short distances traveled during one season. We assume that any change in observed surface velocity from background is due to increased sliding. Accordingly, our velocity data indicate that u_b increases during most of the summer, but we cannot reliably determine the component of the observed background surface velocity due to sliding. Therefore we make an assumption that is conservative for the calculation of $\dot{c}$ as a residual from Equation 5 and assume that during the background time period $u_{b,bg} = u_{s,bg}$, which minimizes the increase in magnitude that we subsequently apply to $u_b \tan\alpha$ during the summer. Because α slopes downward in the direction of flow or is close to zero at all stations, this minimizes our calculation of elevation lowering due to bed parallel motion and, therefore, may underpredict uplift due to $\dot{c}$.

We integrate Equation 5 in time to calculate the displacement due to bed separation, $D_{\dot{c}}$ as a residual using $\Delta t = 1d$

$$D_{\dot{c}} = \dot{c}\Delta t = \Delta z_s - (u_s/u_{s,bg})u_{b,bg}\tan\alpha\Delta t - D_\epsilon \tag{7}$$

where Δz_s is the observed surface displacement.

We estimate the uncertainty in calculated cumulative bed separation to be ~6.5 mm during the background time period, followed by an increase of ~3 mm d^{-1}. By day

191 this results in 10 cm and, by day 223, 20 cm of uncertainty in bed separation (see the Appendix). Additional unquantifiable uncertainty is introduced by assumptions that vertical strain rates are constant with depth, the station pair spacing used for calculating strain rates is appropriate, and uplift due to till dilation is negligible (see the Appendix). For these reasons, we consider the estimated time-series of bed separation to be broadly indicative of increases or decreases in the volume of water stored at the bed, and we consider the relative magnitude and timing to be more reliable than the absolute values.

3. RESULTS AND ANALYSIS

3.1. Seasonal Description

3.1.1. Surface Hydrology

PDD in the region began around day 152 (1 June) and terminated around day 244 (1 September) of 2007 (Figures 2 and 3); the two weather stations reported similar variations in air temperature during the summer. Three prolonged periods of elevated PDD occurred in the middle of the summer: days 175-182, 185-210, and 222-233 (Figure 2). However, due to the upglacier migration of the snowline during the summer (Figure 4), late-summer modeled melt rates tend to be higher. For example, the highest temperatures of the season occurred around day 190. In the downglacier region ice was exposed at this time, leading to the highest modeled melt rates of the summer. In the midglacier and upglacier regions, the highest modeled melt rates occurred during somewhat lower temperatures later in summer as the underlying ice was exposed in those regions. Modeled melt decreased with distance upglacier due to both fewer PDD and prolonged snowcover. Modeled melt for the entire summer was 1.9, 1.1, and 0.4 m w.e. in the downglacier, midglacier and upglacier regions, respectively.

In 2007 there were 15 lakes within 5 km of our GPS stations in our downglacier region, 28 in the midglacier region, and 19 in the upglacier region. Of these 62 lakes, 45 (73%) had a diameter greater than 0.25 km, and 25 (40%) had a diameter greater than 0.50 km. Lake filling in all regions began shortly after the onset of melt and nearly all lakes were identifiable before snowcover became patchy, though lake volume may have continued to increase. Melt rates during lake filling were relatively low compared to melt rates later in the summer after ice was exposed (Figure 2). Within the midglacier and downglacier regions, the peak two-week period of lake draining immediately followed the peak two-week period of lake filling; most lakes persisted for less than a month. In the upglacier region where snowcover remained all summer and modeled melt rates were lower, lake draining occurred over about two months.

3.1.2. Ice Motion

Background velocities prior to the spring speedup (Figures 2) varied from 65 m a^{-1} to 138 m a^{-1} (Table 1) with variations of less than 2% of the mean during the background period. Horizontal trajectories of stations during this period were constant, with maximum across-track displacement less than 5% of daily displacement along the mean trajectory. Prior to day 170, longitudinal strain rates were small ($< 5 \times 10^{-6}$ d^{-1}) and were negative (compressive) throughout most of the area (Figure 5). Over the summer, we observe three modes of velocity change: a seasonal increase associated with the long-term increase in surface melt, diurnal changes, and event-type short-duration increases. Seasonal and event-type motion are best observed when using 24-hour average velocity (Figure 2) while diurnal motion is best observed with 6-hour average velocity (Figure 3).

Summer acceleration in 2007 began in mid to late June as observed in this area by *Zwally et al.* [2002], but the two to four week delay between onset of PDD and onset of acceleration is longer than the zero to two weeks identified previously. The onset of acceleration in the spring occurred later in time at inland stations and migrated inland at an average rate of 30 km and 400 m in elevation over 20 days (Figure 4). After summer speedup, longitudinal strain rates were variable but tended to become more compressive downglacier (e.g. 307/407) and more extensional upglacier (e.g. 607/807) relative to background values (Figure 5). Summer velocity was characterized by sustained, but highly variable, increased speeds, coinciding with periods of modeled melt (Figure 2). Significant seasonal velocity changes were observed at all but the farthest inland station (807).

Average velocities during the ∼40-day period of sustained speedup (days 174-214) were faster than background by 34% in both the downglacier and midglacier regions and by 12% in the upglacier region, with station 107 showing the greatest speedup of 43% (Table 1). The observed summer speedup is comparable to other reports of this phenomenon in west Greenland, given inter-annual variability, varying velocity calculations, and varying definitions of the summer period: At elevations similar to our downglacier stations, *Bartholomew et al.* [2010] observed a 40% increase in velocity during summer. At elevations similar to our midglacier stations, *Zwally et al.* [2002] measured a summer increase in velocity of 12-28%, *Joughin et al.* [2008] an increase of 50%, and *Shepherd et al.* [2009] an increase of about 50%. Over broader areas of the region, *Joughin et al.* [2008] found a summer increase of 50-100% and *van de Wal et al.* [2008] an increase of about 50%. The latter three of these studies was conducted in a region ∼ 300 km farther south of our field site where melting is likelier to occur at higher elevations.

At the downglacier and midglacier stations (107-507, Wild1), the timing of the initial speedup occurred during a period with many lake drainage events and low modeled melt (Figure 2). Significant bed separation occurred at all of the downglacier and midglacier stations and begins within days of summer speedup, implying widespread hydrologic connection between the surface and the bed. The magnitude of the acceleration and the contemporaneous bed separation suggests that speedup was caused by local sliding rather than stress coupling to ice downstream of our study area, but we are unable to determine if the water source for enhanced sliding was contemporaneous melt or the release of water stored in lakes. Within the midglacier region, acceleration and bed separation were both rapid at station 407 and the onset of bed separation preceded the onset of acceleration by a few hours (day 175, Figure 2). Acceleration and bed separation were more gradual at stations 507 and Wild1, with bed separation lagging acceleration by about a day. The delayed, gradual acceleration and bed separation at stations 507 and Wild1 may indicate initial connections between the surface and bed were located farther away than at station 407 and that the first phase ($\sim$24 hr) of acceleration was largely driven by flow coupling.

After initial speedup, the downglacier and midglacier stations maintained increased average daily velocity for about a month before a gradual return to background levels near the end of July when modeled melt approaches zero (Figure 4). No data are available for stations in the downglacier region after day 214, but there was a brief acceleration of about 50% above background in the midglacier region, associated with a few days of elevated melt from day 218-226 (Figures 2, 4). At some stations bed separation appears to peak with the maximum summer velocity (e.g. 107, 207, 407), and at all but 507, bed separation reduced or stabilized by day 200, despite continued moderate to high modeled

melt rates. Bed separation estimates after day 200 are not significant at most stations due to cumulative uncertainty in strain thickening and bed parallel motion (Appendix).

Seasonal speedup at upglacier stations occurred within days of the midglacier stations, but the peak speedup magnitude (<50%) was much less than that at the other stations (200-300%). Modeled melt rates during the period of increased summer velocity in the upglacier region (days 177-201) are comparable to those associated with much larger speedups in the midglacier and downglacier stations. However, there are reasons to expect meltwater-induced sliding to be smaller in the upglacier region. First, fewer lake drainages occurred in the upglacier region, and more than half drained after the velocity had returned to near background levels later in summer (after day ∼205). Second, there are likely few (if any) moulins upstream of the equilibrium line [*Catania et al.*, 2008], and hydrologic connection to the bed may be limited in this region.

After day 226, daily velocities for Wild1, 507, 607 and 707 dropped below the background velocity and became highly variable in magnitude and direction (Figures 2, 4). This includes three events where flow direction was temporarily reversed at Wild1 (negative velocity on days 243, 253, and 260 in Figure 2) [cf. *Harrison et al.*, 1986; *Sugiyama et al.*, 2007; *Fudge et al.*, 2009]. Velocity decreases at the upglacier stations during these flow reversals were inversely proportional with distance from Wild1, providing supporting evidence for their authenticity. Average late summer velocities were about 5% below background velocities, compared with the ∼10% observed by *Zwally et al.* [2002] and *Joughin et al.* [2008, Figure 2]. Though the late summer slowdown was more modest than the spring speedup, it lasted substantially longer in 2007. At station Wild1 the late summer slowdown reduced the average velocity from 38% above background for July to 13% aver-

aged over July-September, with similar effects at the other stations with available data. Our measurements ended in late September before a stable winter velocity was reached, but previous studies have shown a gradual increase to relatively constant winter speeds occurring about this time of year [*Zwally et al.*, 2002; *Joughin et al.*, 2008].

3.2. Diurnal Description

Diurnal velocity fluctuations occurred at most stations during periods of sustained above freezing temperatures, but were either muted or absent when air temperature remained close to zero or below (e.g. days 182–188) (Figure 3). The diurnal velocity amplitude was greatest at the downglacier stations, including station 107, which often exhibited an amplitude greater than 100% of background (Figure 3). The midglacier stations rarely experienced an amplitude of more than 50% of the background velocity. In the upglacier region, diurnal variations are only significant during days 192–195. Longer supraglacial flowpaths (combined with persistent snowcover) in the upglacier region may attenuate the pulse-like nature of daily water input, which has been proposed to be important for generating sliding [*Bartholomaus et al.*, 2008; *Schoof*, 2010].

On days that exhibited diurnal velocity variations, downglacier stations experienced daily maximum velocity ∼3.5–4.75 hours after peak air temperature, the mid-glacier stations ∼5–6 hours, and the upglacier stations ∼7–8 hours. (Air temperature reached a daily maximum around 18:00 UTC, about 3 hours after local solar noon, but the timing varied substantially from day to day.) Several mechanisms may contribute to the observed increased lag between maximum air temperature and peak diurnal velocity for progressively inland GPS stations. First, ice is thicker inland and moulin density is reduced [*Catania et al.*, 2008] suggesting that the englacial and supraglacial travel times

are longer. Second, the surface snowpack lasts longer at higher elevations, providing temporary water storage [*Fountain and Walder*, 1998; *Jansson et al.*, 2003]. Third, delayed acceleration may simply be a result of flow coupling.

While the timing of daily maximum air temperature was roughly constant during the season, the timing of daily peak velocity came an hour or two earlier over the course of the summer for most stations. This suggests the evolution of more efficient hydraulic pathways to the bed over the summer, due to some combination of reduction in supraglacial travel time as the snowpack melts and lakes disappear and/or an increase in the number of open connections to the bed (moulins). The lag times we observed are longer than the ∼2 hr lag observed by *Shepherd et al.* [2009] at a site 300 km south during the same summer, suggesting longer and/or less efficient hydrologic pathways in our area.

3.3. Event Description

We identify velocity events that we presume are related to lakes draining (Table 3) because they appeared at only one or a few adjacent stations, lasted about one day, and occurred at times inconsistent with the typical lag behind daily maximum air temperature (Figures 2, 3). There were a total of eleven such events (Table 3), a small fraction (17%) of the 62 lakes observed to drain over the course of the summer in our 550 km^2 study area and slightly less than half of the lakes greater than 0.5 km in diameter that drained. However, the drainage of the only three lakes in our study area with a diameter ¿1 km were associated with by far the largest velocity events recorded (on days 190-191). These events occurred during the highest temperatures of the season and when lakes were draining in all regions. They resulted in a factor of 2-3 increase in daily velocity at stations 307-507 and Wild1, and an increase of greater than 50% at station 607 (Figure 2). Despite such

dramatic transient effects, these presumed lake drainage events accounted for at most 5% of the total summer motion at any station.

Examination of days 190-191 using 2-hr average velocities (Figure 6) reveals three distinct velocity peaks. The first acceleration occurred early on day 190 and strongly affected station 507, with a much smaller impact at stations Wild1, 407, and 607. Maximum velocity was reached nearly simultaneously at all stations around 06:00 UTC, approximately coincident with the minimum air temperature. Analysis of cloud-free 250-m resolution MODIS band 1 imagery shows that a 1.3-km diameter lake located between 607 and 507 (star A in Figure 1) drained between day 189 23:20 UTC and day 190 14:20 UTC. This timing and location are consistent with lake drainage being the cause of the first peak in Figure 6. Though we do not have information about supraglacial or englacial transport of lake water, we presume water reached the bed closer to 507 than 407, Wild1, or 607 since the impact on velocity was twice as large at 507. However, since 507 did not exhibit detectable uplift during this initial event, we expect the location where water reached the bed was at least 1 km away, as measurable surface uplift due to cavity opening is likely to occur over a length scale comparable to the ice thickness [*Anderson et al.*, 2004].

A second, larger peak in velocity is observed at stations 407, Wild1, and 307 starting in the middle of day 190, peaking within three hours of midnight UTC, about 2.5 to 5.5 hours earlier than the peak time of diurnal fluctuations in air temperature for that day. A third peak occurred at Wild1, and possibly 407, four hours later at 02:30 UTC on day 191. Rapid uplift at Wild1 began with the second peak in velocity, reached a maximum of 9 cm, and was reduced by half by the end of the event ($\sim$12:00 on day 191). Rapid uplift at 407 began during peak acceleration, reached a maximum of 15 cm and was sustained

for several days. There were significant diurnal variations in elevation at stations 407 and Wild1 of 3-5 cm that lasted for a few days after the event.

Analysis of MODIS imagery shows that a second lake, ∼1 km in diameter and 1.3 km downglacier of Wild1 (star B in Figure 1), drained between day 190 14:20 UTC and day 191 00:05 UTC, consistent with the second velocity peak and rapid uplift. Prior to the end of day 190 there was a greater maximum velocity at 407 than Wild1, uplift occurring only at 407, and an increase in velocity at 307. This suggests that water from this second lake was transported supraglacially and/or englacially before reaching the bed closer to 407 than Wild1. Additionally, a third lake, 1 km in diameter and 0.5 km upglacier of Wild1 (star C in Figure 1), drained between day 191 00:05 UTC and day 192 23:50 UTC, potentially explaining the final velocity peak and rapid uplift at Wild1. This last drainage appears to have affected velocity primarily at Wild1, suggesting supraglacial and/or englacial transport was minimal.

4. DISCUSSION

4.1. Flow Coupling vs. Local Acceleration

The observations of *Zwally et al.* [2002] generated debate about whether the connection between surface melt and basal sliding could cause a positive feedback between ice sheet mass loss and climate warming [e.g. *Parizek and Alley*, 2004; *Truffer et al.*, 2005; *Price et al.*, 2008]. A fundamentally important detail is whether surface melt reaches the bed locally near the equilibrium line or only lower in the ablation zone. If melt is able to reach the bed anywhere, seasonal acceleration could potentially migrate rapidly inland into the low-slope accumulation zone as climate warms [*Zwally et al.*, 2002; *Parizek and Alley*, 2004] and promote increased flux of ice to the margin, quickly expanding the ablation

zone. However, *Price et al.* [2008] show that the acceleration observed by *Zwally et al.* [2002] could alternatively be explained by stress coupling of ice near the equilibrium line to ice in the ablation zone. Ice in the ablation zone tends to be heavily crevassed and thinner, and lower in elevation, factors that enable moulin formation and access of surface meltwater to the bed. If acceleration is restricted to highly crevassed areas, both the magnitude and potential future migration of acceleration will be limited.

Our dataset provides an opportunity to compare the relative contribution of local sliding and flow coupling to acceleration near the equilibrium line. At the seasonal scale, we see a fairly uniform speedup of 30-40% in the downglacier and miglacier regions (Table 1). According to the model of *Price et al.* [2008], a 30-40% acceleration ∼10 km downstream from Swiss Camp (i.e. near the locations of 507 and Wild1 in the midglacier region) can explain a speedup at Swiss Camp of 8% using a polythermal ice temperature profile and <5% assuming temperate ice [Figure 3 *Price et al.*, 2008]. Model results using relatively stiff polythermal ice predicted a basal velocity that is 80% of the surface velocity observed by *Zwally et al.* [2002] at Swiss Camp, whereas temperate ice required a basal velocity that is 30% of the surface velocity [*Price et al.*, 2008]. The 18% seasonal speedup that we observe at station 607, 10 km inland of Wild1/507, and the 13% speedup at station 707, 18 km inland of Wild1/507 (Table 1), are substantially greater than can be explained solely through flow coupling, assuming either temperate or polythermal ice, and are therefore consistent with a large component of local acceleration into our upglacier region.

Strain rates and bed separation provide support for our interpretation that much of the seasonal speedup in the upglacier region was due to flow coupling with faster flowing ice downglacier. Longitudinal strain rates between the midglacier and upglacier regions

(stations 407/607) switched from compression during the background period to extension for most of the first half of the period of increased velocity (days 177-193). During this period, the elevation of station 607 lowered from its background trajectory by about 5 cm, equal to the calculated strain thinning. Furthermore, velocity variations at station 607 are highly correlated with those in the midglacier region, consistent with flow coupling.

Initial summer speedups at our stations near Swiss Camp (507, Wild1, and 607) are consistent with the results of *Price et al.* [2008], suggesting the first phase of enhanced summer motion was caused by longitudinal flow coupling. On days 174–175, station 407 (7 km downglacier of Swiss Camp) accelerated 40% while stations 507 and Wild1 (near Swiss Camp) accelerated 6% and 12%, respectively, comparing favorably with the 8% to 15% model prediction for this geometry [*Price et al.*, 2008]. Also in good agreement is the subsequent 40% increase in velocity at Wild1 over days 176-178, during which time station 607, 10 km upglacier, accelerated by 10%. Though this is a somewhat different geometry than considered by *Price et al.* [2008], their modeling predicts an increase in velocity of 5% for isothermal ice and 8% for polythermal ice, suggesting that the speedup at 607 at this time was almost entirely due to flow coupling from acceleration downglacier.

However, our data show brief velocity increases at 607 (20% speedup on days 180-181, 35% speedup on day 190) and 707 (20% speedup on day 195) that cannot be explained by longitudinal flow coupling. There is no such comparable acceleration at our farthest inland station (807). In the case of station 707, there was a brief period of sustained uplift from day 195-210 following the speedup (Figure 2). Concurrent with this is an end to the extensional strain rates between the midglacier and upglacier regions (Figure 5) and the only period of the summer that diurnal variations are statistically significant at station

707 (Figure 3). As with the early speedups in the lower regions, these speedups in the upglacier region occurred while substantial snowcover remained locally (Figure 4).

Therefore, although rare, transient sliding events are possible up to 1385 m a.s.l., which is near the upper estimate of the equilibrium line altitude for this part of the ice sheet [*Zwally et al.*, 2002; *Mernild et al.*, 2008]. We suggest that the relative importance of flow coupling and local acceleration may be influenced by the melt extent and intensity in a given year, and note that 2007 was a record melt year in west Greenland [*Mote*, 2007; *Tedesco*, 2007; *Tedesco et al.*, 2008].

4.2. Relationship Between Hydrology and Velocity

At two sites farther south in west Greenland, *Bartholomew et al.* [2010] identified an early summer background phase of constant velocity, a phase of increased velocity correlated with PDD and accompanied by uplift during midsummer, and a late summer phase of surface lowering with increased velocity only during intense melting. *Bartholomew et al.* [2010] infer that the latter two phases are manifestations of the evolution of the subglacial hydrologic system from an inefficient distributed system to an efficient channelized system, similar to the mechanism ascribed to the spring speedup observed on temperate glaciers [e.g. *Iken et al.*, 1983; *Nienow et al.*, 1998; *Anderson et al.*, 2004]. In this mechanism, increases in water storage at the bed drive decreases in the regional effective pressure (ice overburden pressure minus water pressure), which reduce basal drag and result in increased sliding [*Iken*, 1981; *Iken et al.*, 1983; *Kamb et al.*, 1994; *Bartholomaus et al.*, 2008; *Schoof*, 2010]. The evolution of an efficient channelized subglacial hydrologic system requires meltwater inputs to become increasingly larger in order to maintain water pressures and associated sliding. Subglacial channels can enlarge quickly due to melting

along their walls [*Röthlisberger*, 1972], but in the absence of continued pressurization they creep closed over days to weeks under thin (∼100 m) ice or hours under thick (∼1000 m) ice [*Nye*, 1953; *Bartholomaus et al.*, 2008].

In our downglacier and midglacier regions we see a similar summer evolution: after an early summer period of constant velocity, these regions experienced large increases in velocity ($> 50\%$) that were associated with melt intensity and bed separation (days 173-195), followed by a period of increasingly muted velocity response to melt intensity and decreasing or constant bed separation (days 195-215) (Figure 2). The use of a PDD melt model that includes a time-dependent degree-day factor as the surface changes from snow to ice is critical for revealing the evolution of the dynamic response to surface meltwater forcing. (Though using bi-weekly Landsat imagery causes uncertainty in the timing of surface albedo changes, it highlights that above freezing temperatures in late summer when low albedo ice is exposed produce more melt than in early summer.) The periods of above freezing temperatures and exposed ice that generate large melt rates late in the season (e.g. day 205, 223) were associated with much smaller velocities than periods of more modest melting early in summer (e.g. day 178, 190).

The evolution in the dynamic response of the ice sheet to continued meltwater input that we observe is consistent with sliding being driven by changes in storage at the seasonal and event time-scales, as identified for west Greenland [*Das et al.*, 2008; *Bartholomew et al.*, 2010] and elsewhere [e.g. *Iken et al.*, 1983; *Mair et al.*, 2002b; *Bartholomaus et al.*, 2008; *Howat et al.*, 2008]. Changes in estimated bed separation over time (inferred to be primarily subglacial water storage) correlate with the degree of enhanced sliding observed at the seasonal scale in our study area (Figure 7). The fastest velocities occurred during

the most rapid bed separation (e.g. day 175, 190), and slower velocities occurred when the rate of bed separation was close to zero or negative (Figure 7). At the event time scale, the two lake drainages on day 190 affecting stations 407 and Wild1 each exhibited the type of hysteresis between uplift and velocity observed by *Howat et al.* [2008]; peak velocity during these events coincided with the peak rate of increase in bed separation (Figure 6), which is presumably when water pressures reach their maximum [*Howat et al.*, 2008; *Sugiyama et al.*, 2010]. If the volume of stored water rather than rate of change in storage were to control sliding, one would expect to observe the maximum velocity coincident with maximum uplift [*Iken et al.*, 1983]. Instead, maximum uplift lagged maximum velocity by 7 hours in the event at 407 and 11 hours in the event at Wild1 (Figure 6). Additionally, during periods of low melt input and small or negative rates of bed separation, diurnal variations in velocity were muted or absent (days 180-186, 210-213, Figure 3), conditions that presumably occur when diurnal variations in meltwater input are not large enough to pressurize the system and induce further sliding [*Bartholomaus et al.*, 2008].

We hypothesize that it is the daily meltwater pulses to the englacial/subglacial hydrologic system that enhance sliding in summer. The difference between the maximum and minimum velocity on each day is loosely correlated with modeled melt, given the uncertainty in the melt model, and did not decay over the summer (Figure 8). However, the minimum velocity on each day did tend to decrease over the summer, except for brief periods of particularly large water inputs (e.g. melt and lake drainage on days 190-191, renewed melt on days 220-227). Our interpretation is that daily pulses of meltwater cause sliding throughout the summer through the daily pressurization of the subglacial hydrologic system. As the channelized system becomes more efficient over the summer in

response to these pulses, the nighttime cessation in meltwater input result in increasingly lower water pressures and, therefore, less sliding. This is consistent with the importance of diurnal pulses of water in driving sliding in theoretical work [*Schoof*, 2010; *Pimentel and Flowers*, 2010] and observations [*Iken and Bindschadler*, 1986; *Hubbard et al.*, 1995; *Nienow et al.*, 2005; *Bartholomaus et al.*, 2008; *Mair et al.*, 2008].

Despite the presence of a large overdeepening in the downglacier and midglacier regions (Figure 1), we see consistent speedups between the stations located there, at both the seasonal and daily time scales (Figures 2, 3), and evidence for enhanced sliding throughout the region. The overdeepening does not appear to have a dominant effect on the relationship between hydrology and ice dynamics here, as has been observed on some mountain glaciers [*Hooke et al.*, 1989; *Hooke and Pohjola*, 1994; *Jansson*, 1997; *Fountain and Walder*, 1998], and the evolution of the dynamic response to meltwater input appears to be equally rapid throughout the downglacier and midglacier regions.

However, the ice thickness at station 407 ($\sim$1000 m) should result in creep closure of subglacial conduits and subsequent repressurization of the subglacial hydrologic system (leading to renewed rapid sliding) within hours if water pressures in the conduits fall, while at 107, where the ice is less than half as thick, this process would take days [*Bartholomaus et al.*, 2008]. Despite this, we see a similar evolution in dynamic response at all stations in the downglacier and midglacier regions, suggesting that water pressures are never able to lower sufficiently to allow rapid creep closure of subglacial channels. Previous borehole water pressure observations in $\sim$350 m thick ice downstream of our study area measured water pressures of 85-94% of overburden pressure [*Thomsen et al.*, 1991], and in $\sim$850 m thick ice to the south of our study area near Jakobshavns Isbrae measured water pressures

were close to overburden [*Lüthi et al.*, 2002]. Thus, it appears likely that despite the thick ice encountered in parts of the ablation zone in west Greenland, the ice sheet hydrology is similar to that of thinner glaciers due to the existence of similar effective pressures during much of summer.

However, the increased ice thickness may contribute to the high variability in velocity (10-50%) observed in late summer when surface melt and lake drainages have ended (after day 243, Figure 2). Effective pressure is likely to be substantially higher after water input stops and stored water has drained, increasing basal drag. Additionally, if cavities become isolated from the subglacial hydrologic system, they reduce the extent to which variations in water pressure are transmitted across the bed, creating 'sticky spots' that reduce sliding and surface velocity [*Iken and Truffer*, 1997; *Mair et al.*, 2001], which could explain the episodes when velocity dips substantially below background levels. Furthermore, *Balise and Raymond* [1985] showed that as the spatial extent of sliding is reduced below about ten ice thicknesses, the expression at the surface of basal velocity changes can be dramatically reduced, and even negative under certain circumstances.

4.3. Dynamic Effects of Supraglacial Lake Drainages

Das et al. [2008] observed drainage of a ∼2-km diameter lake to the base of the ice sheet in less than 2 hours through fractures in the lake floor. A GPS station placed 0.5 km from the lake edge measured a peak across-flow velocity that was 100 times the background velocity and coincident rapid uplift of 1.2 m. The velocity events we observed on days 190–191 (Figure 6) were of similar duration (∼0.5 d) and show a qualitatively similar ice dynamic response but with reduced magnitudes of velocity and uplift. We observed a velocity change that is ∼4 times the background velocity at station 507 and ∼5 times

the background velocity at stations 407 and Wild1 with uplifts that were about an order of magnitude less than observed by *Das et al.* [2008]. Further, we did not observe the large lateral translation of our GPS receiver during the largest lake drainage events as observed by *Das et al.* [2008]. These differences are likely because our GPS stations were located along the flow direction relative to lake position, rather than perpendicular to the flow direction as in the case of *Das et al.* [2008]. Additionally, our GPS stations were at greater distances away from the lakes, causing a muted response. As observed by *Das et al.* [2008], lake drainages appear to have little lasting effect on ice dynamics with ice velocities returning to values from prior to the event within a day. This is further evidence of the existence of efficient channelized drainage by mid-summer, which is consistent with modeling of such a system [*Pimentel and Flowers*, 2010].

The rare occurrence of velocity events related to lake drainage is supported by previous studies that identify one or two clear events per summer in GPS records [*Joughin et al.*, 2008; *van de Wal et al.*, 2008; *Bartholomew et al.*, 2010]. That we did not detect velocity events associated with the draining of many of the smaller lakes suggests that either their impact was local enough that it was undetectable by our GPS array or that they did not significantly enhance sliding. However, given our ability to detect longitudinal coupling between stations associated with moderate acceleration (50%) as described above, it is likely that lake drainage events an order of magnitude smaller than the three described in detail (Figure 6) would also be detectable within our network. Explanations for the relative lack of observed acceleration events include: 1) Lakes that drain slowly by over-topping or breaching their outlet and emptying overland into streams before reaching a crevasse or moulin would not generate a large pulse of water. The lack of correlation

between moulin and lake locations supports this [*Catania et al.*, 2008]. Lakes that drain over days to weeks may deliver diurnal pulses of water to the subglacial hydrologic system that are similar to those from direct input of supraglacial streams. 2) Some lake drainages may appear as large diurnal fluctuations and escape detection since lakes may be more likely to drain during times of peak melting when lake levels are rising. 3) Water draining into crevasses rather than moulins may be attenuated or refrozen englacially before contributing to the subglacial hydrologic system [*McGrath et al.*, 2011]. 4) Finally, an efficient subglacial drainage system may be capable of accommodating moderate lake drainages such that peak water pressures are reduced and the impact on surface velocities is small and spatially localized [*Pimentel and Flowers*, 2010]. Better constraints on the timing, duration, and volume of lake drainage events may help identify the processes affecting smaller lake drainages.

5. CONCLUSIONS

Similar to previous studies [*Zwally et al.*, 2002; *Joughin et al.*, 2008; *van de Wal et al.*, 2008; *Shepherd et al.*, 2009; *Bartholomew et al.*, 2010; *Sundal et al.*, 2011; *Palmer et al.*, 2011], we observed an early summer background period of constant ice velocity in west Greenland, followed by a speedup that lasted most of the summer and was associated with surface melt (Figure 2). We also observed uplift and diurnal velocity variations that occurred throughout most of the summer (Figures 2, 3). Local acceleration due to enhanced basal sliding appears to be responsible for most of the observed speedup, but longitudinal flow coupling can explain many (but not all) of the smaller variations in ice motion observed near the equilibrium line. Areas in the ablation zone typically experienced one to two velocity events that are inferred to result from supraglacial lake

drainage, but in all cases the effects are short-lived (<1 d) and local (<10 km). Drainages of the three lakes in our study area that were >1 km in diameter produced dynamic responses comparable to previous observations of lake drainage [*Das et al.*, 2008], but less than half of drainages from lakes >0.5 km in diameter were detected in our data. Thus, direct input of runoff and supraglacial streams to moulins seems to be far more important for the seasonal velocity response than catastrophic lake drainage or flow coupling [*Gulley et al.*, 2009].

Our data substantiate the growing evidence collected 300 km to the south [*Bartholomew et al.*, 2010; *Sundal et al.*, 2011; *Bartholomew et al.*, 2011] that the dynamic response of the Greenland Ice Sheet to meltwater input markedly evolves over the course of the summer. Across our downglacier and midglacier regions, the increase in velocity above background levels tends to be lower in late summer than in early summer, despite similar above-freezing air temperatures and the expected increase in melt rates due to the transition from a snow to ice surface (Figure 2). We attribute the change in dynamic response to the formation of a subglacial channel network capable of efficiently transporting water under the ice sheet. We see evidence at the seasonal (Figure 2) and event scales (Figure 6) that sliding is driven by changes in storage, as has been interpreted for mountain glaciers [*Iken et al.*, 1983; *Kamb et al.*, 1994; *Bartholomaus et al.*, 2008; *Schoof*, 2010]. Despite the presence of thick ice (∼1000 m), the hydrology of our study area behaves qualitatively similar to that of mountain glaciers, and it appears likely that sustained storage of water in the ice sheet maintains effective pressure similar to mountain glaciers for much of summer. Higher effective pressures late in summer after melt input has ceased and stored water

has substantially drained may help explain the high variability in velocity observed in late summer, including flow reversals.

Our observations support the ideas that rising air temperatures in Greenland may not translate directly into increased sliding at the seasonal scale [*Truffer et al.*, 2005; *van de Wal et al.*, 2008; *Bartholomew et al.*, 2010; *Schoof*, 2010; *Sundal et al.*, 2011] and that episodic pulses of water are key for generating enhanced sliding [*Bartholomaus et al.*, 2008; *Schoof*, 2010]. Daily pulses of meltwater appear to cause variations in daily sliding that are broadly consistent over space and time in our study area, but these daily increases in velocity are superimposed on a nighttime velocity that generally decreases over the season, presumably as the subglacial hydrologic system becomes more efficient (Figure 8). Thus, accurately predicting future dynamics of the ice sheet in response to changes in surface melt may require knowledge of both melt generation and the state of the subglacial hydrologic system at high temporal resolution.

6. Appendix: Assessment of Uncertainty in Bed Separation

Uncertainty in our calculations of bed separation is due to measurement uncertainty in the vertical positions measured by GPS (∼5 mm), assumptions and quantifiable uncertainty in calculations of vertical strain rate and bed parallel motion, and the contribution of till dilation to $\dot{c}$.

The quantifiable uncertainty in strain rate is $\sqrt{2}\sigma_l(l\Delta t)^{-1}$, where σ_l is the uncertainty in the baseline length between stations (∼6 mm), which corresponds to 2×10^{-6} d^{-1} for the 4 km baseline between stations 107 and 207 and 5×10^{-7} d^{-1} for the 17 km baseline between stations 407 and 607. Assuming an uncertainty in ice thickness of 50 m, error propagation through Equation 4 results in quantifiable uncertainty in D_ϵ of 0.7 mm d^{-1}

and 1.0 mm d^{-1} for the baselines between 407/607 (H=1000 m) and 107/207 (H=500 m), respectively. Additional uncertainty in strain rate comes from assuming that: 1) lateral strain is zero, 2) vertical strain rates are constant with depth, and 3) the station pair spacing used is appropriate (Table 2).

We assess assumption 1 using calculations of lateral strain rate between stations 507 and Wild1. The lateral strain rate between stations 507/Wild1 is an order of magnitude lower than the longitudinal strain rate between stations 407/607 prior to the local onset of enhanced summer motion (day 173) (Figure 5). Assuming lateral strain between 507/Wild1 is representative of the entire study area, ignoring lateral strain may affect calculations of background vertical strain by 3×10^{-7} d^{-1}, which corresponds to uncertainty in D_ϵ of 1.0 mm d^{-1} and 0.5 mm d^{-1} for station pairs 107/207 and 407/607, respectively. However, lateral strain between 507/Wild1 is an order of magnitude larger during summer, and this results in uncertainty in D_ϵ increasing to 3.0 mm d^{-1}.

Hooke et al. [1989] and *Mair et al.* [2002b] make detailed assessments of the uncertainty in bed separation introduced by assuming that the vertical strain rate is constant with depth (assumption 2). Instead, we assume the vertical strain rate is constant with depth and acknowledge that this assumption may introduce unknown errors into our calculation of bed separation [*Anderson et al.*, 2004; *Howat et al.*, 2008]. However, we find, like *Anderson et al.* [2004], that actual depth-averaged vertical strain rates would have to be several times larger than the values we calculate from surface observations in order to make our calculations of bed separation insignificant (e.g. Figure 9).

Finally, the choice of baseline length with which to calculate strain rates introduces uncertainty. For a hydrological study of an alpine glacier, *Mair et al.* [2002b] advocate for

calculations over a longitudinal length-scale of 5H. Here we use baseline lengths between 10 and 21 ice thicknesses, with the exception of the two end stations which are shorter (Table 2), which is somewhat longer than the theoretical longitudinal coupling length for ice sheets of 4-10H [*Kamb and Echelmeyer*, 1986]. However, we suggest it is preferable to use along-flow baselines that extended both up and downstream of each station where possible. Given our network, some baselines are not centered on the stations they are meant to represent, and this introduces additional uncertainty which we are unable to quantify.

The vertical component of bed parallel motion during the background period is calculated as a residual from the observations of vertical motion (uncertainty of $\sim$0.35 mm d^{-1} over a 20 day period) and calculations of background vertical strain, with a resulting uncertainty of 0.8-1.1 mm d^{-1} (e.g. Figure 9). During the summer, there is additional uncertainty in the vertical component of bed parallel motion due to changes in u_b, but as described in Section 2.5 we make an assumption regarding changes in u_b that is conservative for calculations of $\dot{c}$.

When applying these uncertainties to Equation 7 for calculating bed separation for each day, uncertainty in the measured elevation is assumed constant at 5 mm, while assumed uncertainty due to strain thickening/thinning is cumulative at 3 mm d^{-1} and assumed uncertainty due to bed parallel motion is cumulative at 1 mm d^{-1}. Propagating these uncertainties through Equation 7 results in uncertainty in $\dot{c}$ of 6.5 mm at the end of the background time period with an increase of about 3 mm d^{-1} (Figure 9). By day 191 this results in 10 cm and, by day 223, 20 cm of uncertainty in bed separation. Subglacial till dilation may contribute to $\dot{c}$ and introduces uncertainty in our interpretation of $\dot{c}$ as

bed separation due to storage of water subglacially. However, we expect the effect of till dilation to be small because uplift on the order of 10 cm from till dilation alone would require dilation of a till layer thicker than ∼4 m [*MacGregor et al.*, 2005; *Iken et al.*, 1983].

Acknowledgments. We thank VECO, Michelle Koutnik and Jamin Greenbaum for assistance in the field, Koni Steffen's group at the Cooperative Insitute for Research in Environmental Sciences (CIRES) for providing GC-Net weather data, Matt King for advice on processing the GPS data, and Jamie Clark for assistance with Landsat imagery. This work was funded by NASA Grant NNG06GA83G to Neumann and Catania. Landsat data are distributed by the U.S. Geological Survey (USGS) Earth Resources Observation and Science (EROS) Center, and MODIS data are distributed by the Land Processes Distributed Active Archive Center (LP DAAC), located at the USGS EROS Center (lpdaac.usgs.gov). We thank three anonymous reviewers for their thoughtful, in-depth reviews that substantially improved the manuscript.

References

Ahlstrøm, A. P. (2007), Previous glaciological activities related to hydropower at Paakitsoq, Ilulissat, West Greenland, *Tech. Rep. 25*, Geological Survey of Denmark and Greenland.

Andersen, M., M. Nettles, P. Elosegui, T. Larsen, G. Hamilton, and L. Stearns (2011), Quantitative estimates of velocity sensitivity to surface melt variations at a large Greenland outlet glacier, *Journal of Glaciology*, *57*, 609–620.

Andersen, M. L., et al. (2010), Spatial and temporal melt variability at Helheim Glacier, East Greenland, and its effect on ice dynamics, *Journal of Geophysical Research*,

115(F4), F04,041.

Anderson, R. S., S. Anderson, K. MacGregor, E. Waddington, S. O'Neel, C. Riihimaki, and M. Loso (2004), Strong feedbacks between hydrology and sliding of a small alpine glacier, *Journal of Geophysical Research*, *109*(F03005), 10.1029/2004JF000,120, doi: 10.1029/2004JF000120.

Balise, M., and C. F. Raymond (1985), Transfer of basal sliding variations to the surface of a linearly viscous glacier, *Journal of Glaciology*, *31*(109), 308–318.

Bamber, J. L., S. Ekholm, and W. Krabill (2001), A new, high resolution digital elevation model of Greenland fully validated with airborne laser altimeter data, *Journal of Geophysical Research*, *106*(B4), 6733–6745.

Bamber, J. L., R. B. Alley, and I. Joughin (2007), Rapid response of modern day ice sheets to external forcing, *Earth and Planetary Science Letters*, *257*(1-2), 1–13, doi: 10.1016/j.epsl.2007.03.005.

Bartholomaus, T., R. S. Anderson, and S. Anderson (2008), Response of glacier basal motion to transient water storage, *Nature Geoscience*, *1*, 33–37.

Bartholomew, I., P. Nienow, D. Mair, A. Hubbard, M. A. King, and A. Sole (2010), Seasonal evolution of subglacial drainage and acceleration in a Greenland outlet glacier, *Nature Geoscience*, *3*, 408–411.

Bartholomew, I., P. Nienow, A. Sole, D. Mair, T. Cowton, S. Palmer, and J. Wadham (2011), Supraglacial forcing of subglacial drainage in the ablation zone of the Greenland Ice Sheet, *Geophysical Research Letters*, *38*, L08,502.

Box, J. E., and K. Ski (2007), Remote sounding of Greenland supraglacial melt lakes: implications for subglacial hydraulics, *Journal of Glaciology*, *53*(181), 257–265.

Braithwaite, R., and O. Olesen (1987), Calculation of glacier ablation from air temperature, West Greenland, *Glacier Fluctuations and Climate Change*, *Kluwer*(Dordrect, Netherlands), 219–233.

Braithwaite, R. J. (1995), Positive degree-day factors for ablation on the Greenland ice sheet studied by energy-balance modelling, *Journal of Glaciology*, *41*, 153–160.

Catania, G. A., and T. A. Neumann (2010), Persistent englacial drainage features in the Greenland Ice Sheet, *Geophysical Research Letters*, *37*(L02501), 10.1029/2009GL041,108, doi:10.1029/2009GL041108.

Catania, G. A., T. Neumann, and S. F. Price (2008), Characterizing englacial drainage in the ablation zone of the Greenland Ice Sheet, *Journal of Glaciology*, *54*(187), 567–578.

Chen, G. (1998), GPS kinematic positioning for airborne laser altimetry at Long Valley, California, *Ph.D. Thesis*, *Mass. Inst. of Tech.*(Cambridge, MA).

Choi, K., A. Bilich, K. M. Larson, and P. Axelrad (2004), Modified sidereal filtering: Implications for high-rate GPS positioning, *Geophysical Research Letters*, *31*, L22,608.

Das, S. B., I. Joughin, M. D. Behn, I. M. Howat, M. A. King, D. Lizarralde, and M. Bhatia (2008), Fracture propagation to the base of the Greenland Ice Sheet during supraglacial lake drainage, *Science*, *320*, 778–781, doi:doi:10.1126/science.1153360.

Fausto, R. S., A. P. Ahlstrm, D. van As, S. J. Johnsen, P. L. Langen, and K. Steffen (2009), Improving surface boundary conditions with focus on coupling snow densification and meltwater retention in large-scale ice-sheet models of Greenland, *Journal of Glaciology*, *55*, 869 – 878.

Fountain, A. G., and J. S. Walder (1998), Water flow through temperate glaciers, *Reviews of Geophysics*, *36*(3), 299–328.

Fudge, T., J. T. Harper, N. F. Humphrey, and W. Pfeffer (2009), Rapid glacier sliding, reverse ice motion and subglacial water pressure during an autumn rainstorm, *Journal of Glaciology*, *50*, 101 –108.

Gudmundsson, H. (2003), Transmission of basal variability to a glacier surface, *Journal of Geophysical Research*, *108(B5)*, 2253.

Gulley, J., D. I. Benn, E. Screaton, and J. Martin (2009), Mechanisms of englacial conduit formation and their implications for subglacial recharge, *Quaternary Science Reviews*, *28*(19-20), 1984–1999, doi:10.1016/j.quascirev.2009.04.002.

Harper, J. T., N. F. Humphrey, W. T. Pfeffer, and B. Lazar (2007), Two modes of accelerated glacier sliding related to water, *Geophysical Research Letters*, *34*(L12503), doi:10.1029/2007GL030233.

Harrison, W., C. Raymond, and P. MacKeith (1986), Short period motion events on Variegated Glacier as observed by automatic photography and seismic methods, *Annals of Glaciology*, *8*, 82–89.

Hooke, R. L., and V. A. Pohjola (1994), Hydrology of a segment of a glacier situated in an overdeepening, Storglaciären, Sweden, *Journal of Glaciology*, *40*, 140–148.

Hooke, R. L., P. Calla, P. Nilsson, and M. Stroeven (1989), A three-year record of seasonal variations in surface velocity, Storglaciären, Sweden, *Journal of Glaciology*, *35*(120), 235–247.

Howat, I. M., S. Tulaczyk, E. Waddington, and H. Bjornsson (2008), Dynamic controls on glacier basal motion inferred from surface ice motion, *Journal of Geophysical Research*, *113*(F03015), 10.1029/2007JF000,925, doi:10.1029/2007JF000925.

Howat, I. M., J. E. Box, Y. Ahn, A. Herrington, and E. M. McFadden (2010), Seasonal variability in the dynamics of marine-terminating outlet glaciers in Greenland, *Journal of Glaciology*, *56*, 601–613.

Hubbard, B., M. J. Sharp, I. C. Willis, M. K. Nielsen, and C. Smart (1995), Borehole water-level variations and the structure of the subglacial hydrological system of Haut Glacier d'Arolla, Valais, Switzerland, *Journal of Glaciology*, *41*(139), 572–583.

Iken, A. (1981), The effect of the subglacial water pressure on the sliding velocity of a glacier in an idealized numerical model, *Journal of Glaciology*, *27*(97), 407–421.

Iken, A., and R. Bindschadler (1986), Combined measurements of subglacial water pressure and surface velocity of Findelengletscher, Switzerland: Conclusions about drainage system and sliding mechanism, *Journal of Glaciology*, *32*(110), 101–119.

Iken, A., and M. Truffer (1997), The relationship between subglacial water pressure and velocity of Findelengletscher, Switzerland, during its advance and retreat, *Journal of Glaciology*, *43*(144), 328–338.

Iken, A., H. Röthlisberger, A. Flotron, and W. Haeberli (1983), The uplift of the Unteraargletscher at the beginning of the melt season – a consequence of water storage at the bed?, *Journal of Glaciology*, *29*(101), 28–47.

Jansson, P. (1997), Longitudinal coupling in ice flow across a subglacial ridge, *Annals of Glaciology*, *24*, 169–174.

Jansson, P., R. Hock, and T. Schneider (2003), The concept of glacier storage: a review, *Journal of Hydrology*, *282*, 116–129.

Joughin, I., S. B. Das, M. A. King, B. E. Smith, I. M. Howat, and T. Moon (2008), Seasonal speedup along the western flank of the Greenland Ice Sheet, *Science*, *320*(5877),

781–783, doi:10.1126/science.1153288.

Kamb, B., and K. A. Echelmeyer (1986), Stress-gradient coupling in glacier flow: I. Longitudinal averaging of the influence of ice thickness and surface slope, *Journal of Glaciology*, *32*(111), 267–284.

Kamb, B., H. Engelhardt, M. A. Fahnestock, N. F. Humphrey, M. F. Meier, and D. B. Stone (1994), Mechanical and hydrologic basis for the rapid motion of a large tidewater glacier. 2: Interpretation, *Journal of Geophysical Research*, *99*(B8), 15,231–15,244.

Lüthi, M. P., M. Funk, A. Iken, S. Gogineni, and M. Truffer (2002), Mechanisms of fast flow in Jakobshavns Isbrae, Greenland; Part III: Measurements of ice deformation, temperature and cross-borehole conductivity in boreholes to the bedrock, *Journal of Glaciology*, *48*(162), 369–385.

MacGregor, K., C. Riihmiaki, and R. Anderson (2005), Spatial and temporal evolution of rapid basal sliding on Bench Glacier, Alaska, USA, *Journal of Glaciology*, *51*, 49–63.

Mair, D., P. Nienow, I. WIllis, and M. Sharp (2001), Spatial patterns of glacier motion during a high-velocity event: Haut Glacier d'Arolla, Switzerland, *Journal of Glaciology*, *47*(156), 9–20.

Mair, D., P. Nienow, M. Sharp, T. Wohlleben, and I. Willis (2002a), Influence of subglacial drainage system evolution on glacier surface motion: Haut Glacier d'Arolla, Switzerland, *Journal of Geophysical Research*, *107(B8)*, 2175.

Mair, D., M. J. Sharp, and I. C. Willis (2002b), Evidence for basal cavity opening from analysis of surface uplift during a high-velocity event: Haut Glacier d'Arolla, Switzerland, *Journal of Glaciology*, *48*(161), 208–216.

Mair, D., B. Hubbard, P. Nienow, I. Willis, and U. H. Fischer (2008), Diurnal fluctuations in glacier ice deformation: Haut Glacier d'Arolla, Switzerland, *Earth Surface Processes and Landforms*, *33*, 1272–1284.

McGrath, D., W. Colgan, K. Steffen, P. Lauffenburger, and J. Balog (2011), Assessing the summer water budget of a moulin basin in the Sermeq Avannarleq ablation region, Greenland Ice Sheet, *Journal of Glaciology*, *57*, 954–964.

Mernild, S. H., G. E. Liston, C. A. Hiemstra, and K. Steffen (2008), Surface melt area and water balance modeling on the Greenland Ice Sheet 1995-2005, *Journal of Hydrometeorology*, *9*, 1191–1211.

Mote, T. L. (2007), Greenland surface melt trends 1973–2007: Evidence of a large increase in 2007, *Geophysical Research Letters*, *34*(L22507), doi:10.1029/2007GL031976.

Nienow, P., M. J. Sharp, and I. C. Willis (1998), Seasonal changes in the morphology of the subglacial drainage system, Haut Glacier D'Arolla, Switzerland, *Earth Surface Processes and Landforms*, *23*, 825–843.

Nienow, P. W., A. L. Hubbard, B. P. Hubbard, D. M. Chandler, D. W. F. Mair, M. J. Sharp, and I. C. Willis (2005), Hydrological controls on diurnal ice flow variability in valley glaciers, *Journal of Geophysical Research*, *110*, F04,002.

Nye, J. F. (1953), The flow law of ice from measurements in glacier tunnels, laboratory experiments and the Jungfraufirn borehole experiment, *Proceedings of the Royal Society A: Mathematical*, *219*(1193), 477–489.

Palmer, S., A. Shepherd, P. Nienow, and I. Joughin (2011), Seasonal speedup of the Greenland Ice Sheet linked to routing of surface water, *Earth and Planetary Science Letters*, *302*, 423–428.

Parizek, B. R., and R. B. Alley (2004), Implications of increased Greenland surface melt under global-warming scenarios: ice-sheet simulations, *Quaternary Science Reviews*, *23*(9-10), 1013–1027, doi:10.1016/j.quascirev.2003.12.024.

Pimentel, S., and G. E. Flowers (2010), A numerical study of hydrologically driven glacier dynamics and subglacial flooding, *Proceedings of the Royal Society A*, *467*, 537–558.

Price, S. F., A. J. Payne, G. A. Catania, and T. Neumann (2008), Seasonal acceleration of inland ice via longitudinal coupling to marginal ice, *Journal of Glaciology*, *54*(185), 213–219.

Röthlisberger, H. (1972), Water pressure in intra– and subglacial channels, *Journal of Glaciology*, *11*(62), 177–203.

Rumrill, J. (2009), Analysis of Spatial and Temporal Variations in Strain Rates Near Swiss Camp, Greenland, Master's thesis, University of Vermont.

Schoof, C. (2010), Ice-sheet acceleration driven by melt supply variability, *Nature*, *468*, 803–806, doi:10.1038/nature09618.

Shepherd, A., A. L. Hubbard, P. Nienow, M. A. King, M. Mcmillan, and I. Joughin (2009), Greenland ice sheet motion coupled with daily melting in late summer, *Geophysical Research Letters*, *36*(L01501), 10.1029/2008GL035,758, doi:10.1029/2008GL035758.

Steffen, K., and J. E. Box (2001), Surface climatology of the Greenland ice sheet: Greenland Climate Network 1995-1999, *Journal of Geophysical Research*, *106*(D24), 33,951 – 33,964.

Sugiyama, S., and H. Gudmundsson (2004), Short-term variations in glacier flow controlled by subglacial water pressure at Lauteraargletscher, Bernese Alps, Switzerland, *Journal of Glaciology*, *50*(170), 353–362.

Sugiyama, S., A. Bauder, P. Weiss, and M. Funk (2007), Reversal of ice motion during the outburst of a glacier-dammed lake on Gornergletscher, Switzerland, *Journal of Glaciology*, *53*(181), 172–180.

Sugiyama, S., A. Bauder, P. Riesen, and M. Funk (2010), Surface ice motion deviating toward the margin during speed-up events at Gornergletscher, Switzerland, *Journal of Geophysical Research*, *115*, F03,010.

Sundal, A. V., A. Shepherd, P. Nienow, E. Hanna, S. Palmer, and P. Huybrechts (2011), Melt-induced speed-up of Greenland ice sheet offset by efficient subglacial drainage, *Nature*, *469*, 521–524.

Tedesco, M. (2007), A new record in 2007 for melting in Greenland, *EOS, Transactions of the American Geophysical Union*, *88*, doi:10.1029/2007EO390,003.

Tedesco, M., M. Serreze, and X. Fettweis (2008), Diagnosing the extreme surface melt event over southwestern Greenland in 2007, *The Cryosphere*, *2*, 159–166.

Thomsen, H., O. Olesen, R. J. Braithwaite, and C. Boggild (1991), Ice drilling and mass balance at Pakitsoq, Jakobshavn, central West Greenland, *Rapport Gronlands Geologiske Undersogelse*, *152*, 80–84.

Truffer, M., W. D. Harrisson, and R. March (2005), Record negative glacier balances and low velocities during the 2004 heatwave in Alaska, USA: Implications for the interpretation of observations by Zwally and others in Greenland, *Journal of Glaciology*, *51*(175), 663–664.

van de Wal, R., W. Boot, M. R. van den Broeke, C. J. P. P. Smeets, C. H. Reijmer, J. J. A. Donker, and J. Oerlemans (2008), Large and rapid melt-induced velocity changes in the ablation zone of the Greenland Ice Sheet, *Science*, *321*(5885), 111–113, doi:

10.1126/science.1158540.

van de Wal, R. S. E. (1996), Mass-balance modelling of the Greenland ice sheet: A comparison of an energy-balance model and a degree-day model, *Annals of Glaciology*, *23*, 36–45.

Zwally, H. J., W. Abdalati, T. Herring, K. M. Larson, J. Saba, and K. Steffen (2002), Surface melt-induced acceleration of Greenland Ice-Sheet flow, *Science*, *297*(5579), 218–222.

Site	Dist. from term. (km)	Elev. (m)	Ice thick. (m)	Background vel. (m a^{-1})	Speed-up through 1 Aug	Slowdown after 1 Aug
107	28.0	849	400	65.5	41%	n/a
207	32.0	920	572	64.7	31%	n/a
307	33.5	955	748	100.0	32%	n/a
407	40.0	1044	1058	102.3	37%	n/a
Wild1	46.0	1118	883	75.0	38%	4%
507	48.0	1135	925	137.8	31%	n/a
607	56.5	1225	1091	110.8	18%	5%
707	64.0	1385	1216	110.5	13%	3%
807	69.5	1388	1194	125.6	6%	2%

Table 1. Summary of measurements at all stations. Speed-up and slowdown are averages for their respective time periods and are relative to background velocity. Ice thickness derived from *Catania et al.* [2008].

Site	Baseline endpoints	Baseline length, l_o (km)	l_o/H
107	107, 207	3.7	9.3
207	107, 407	12.0	21.0
307	107, 407	12.0	16.0
407	207, Wild1	14.7	13.9
Wild1	407, 607	17.1	19.4
507	407, 607	17.1	18.5
607	Wild1, 707	18.8	17.2
707	607, 807	12.6	10.4
807	707, 807	6.0	5.0

Table 2. Baselines used for longitudinal strain rate calculations at each station.

day	107	207	307	407	Wild1	507	607	707	807
162	1.6/4	–	–	–	–	–	–	–	–
168	1.5/n	–	–	–	–	–	–	–	–
175	–	–	–	1.5/8	–	–	–	–	–
178	–	–	2.2/4	–	–	–	–	–	–
182 00:00	2.0/n	1.9/n	2.0/n	–	–	–	–	–	–
182 19:00	–	–	–	–	–	2.3/n	–	–	–
183	1.8/n	1.5/n	2.0/n	–	–	–	–	–	–
190 06:00	–	–	–	–	–	3.5/n	1.7/n	–	–
190 22:00	–	–	2.8/n	3.8/15	3.8/n	–	–	–	–
191 03:00	–	–	–	–	4.0/9	–	–	–	–
195	–	–	–	–	–	–	–	1.6/4	–

Table 3. Event-type motion occurring in 2007, defined as acceleration occurring at times of low PDD. First value in each entry indicates the peak 6-hour average velocity relative to background that occurred during the event. Second value indicates the amount of uplift (in cm) associated with the event, with 'n' indicating negligible uplift. Entries with dashes indicate that no event was detected at that station on that day.

Figure 1. Landsat ETM image from 1 August, 2001 showing locations of GPS stations (red triangles), weather stations (green squares), and lakes (blue circles). Open/filled circles indicate lakes that drained/filled during the June 22–July 8, 2007 time period. Large grey circles indicate the 5 km buffers around each GPS station used for lake statistics. Surface elevation contours from *Bamber et al.* [2001]. Locations of bedrock-mounted base stations used in this study (KAGA, KELY and KULU) are shown in the inset map of Greenland. Yellow stars indicate lakes that drained between days 190–192 ordered chronologically from A to C, as detected from MODIS imagery (Figure 6). Inset shows ice sheet surface and bed elevation [*Catania et al.*, 2008] along the GPS station flowline.

Figure 2. Modeled melt (gray), 24-hr mean horizontal velocity (dark blue, green, and red lines) and estimated bed separation (light blue, green, and red lines) for GPS stations. Top: Stations 107, 207 and 307 overlying modeled melt from JAR1. Middle: Stations 407, 507 and Wild1 overlying modeled melt from Swiss Camp. Bottom: Stations 607, 707 and 807 overlying modeled melt based on hourly temperatures extrapolated to mean elevation in this region. Velocity has been normalized with respect to the background velocity (Table 1) at the beginning of the data collection period (days 133–158). Number of lakes filling and draining during each Landsat imagery time period within each region are indicated at the top of each frame.

Figure 3. 6-hr mean horizontal velocity (dark blue, green, and red lines) and hourly air temperature (gray) for GPS stations. Top: Stations 107, 207 and 307 overlying temperature from JAR1. Middle: Stations 407, 507 and Wild1 overlying temperature from Swiss Camp. Bottom: Stations 607, 707 and 807 overlying temperatures extrapolated to mean elevation in this region. Velocity has been normalized with respect to the background velocity (Table 1) at the beginning of the data collection period (days 133–158). Note the change in horizontal and vertical scales from Figure 2.

Figure 4. Normalized 24-hr average velocity change from background with distance from terminus over time. Black contours indicate velocity 5% greater than background, and gray contours indicate velocity 5% less than background. White areas indicate missing data, including the extended period after day 217 across the lower half of the study area. The location of the boundary between continuous and patchy snow is shown with a solid magenta line, and the boundary between patchy snow and ice is shown with a dotted magenta line. Relative PDD at Swiss Camp is shown at the bottom for reference.

Figure 5. Mean daily strain rates. Longitudinal strain rates between 307/407 (blue), 407/607 (green), and 607/807 (red), lateral strain rate between 507/Wild1 (black), and vertical strain rate approximately at Swiss Camp (gray). Additional baselines are in *Rumrill* [2009].

Figure 6. 2-hour average velocity normalized by background velocity for the large events on days 190–191. Dashed lines show elevation change for stations 407 (black) and Wild1 (red). Thin vertical dashed lines represent dates when MODIS imagery is available and is used to identify when lakes drain.

Figure 7. Time series of normalized velocity deviation (increase in velocity above background level) in black and rate of bed separation ($\dot{c}$) in gray for a) station 107, b) station 407.

Figure 8. Minimum daily velocity (black) and difference between maximum and minimum daily velocity (dark gray) for stations a) 107 and b) 407. The mean 6-hr velocity time-series is used. Also shown in light gray is modeled melt at a) JAR1 and b) Swiss Camp.

Figure 9. Example of calculation of components of vertical motion,w_s (black, measured by GPS), at Wild1: bed parallel motion, $u_b \tan \alpha$ (dark gray); strain thickening/thinning, $\dot{\epsilon}_{zz} H$ (dashed dark gray); and bed separation, $\dot{c}$ (light gray). Uncertainty in bed separation is shown with dotted gray lines.

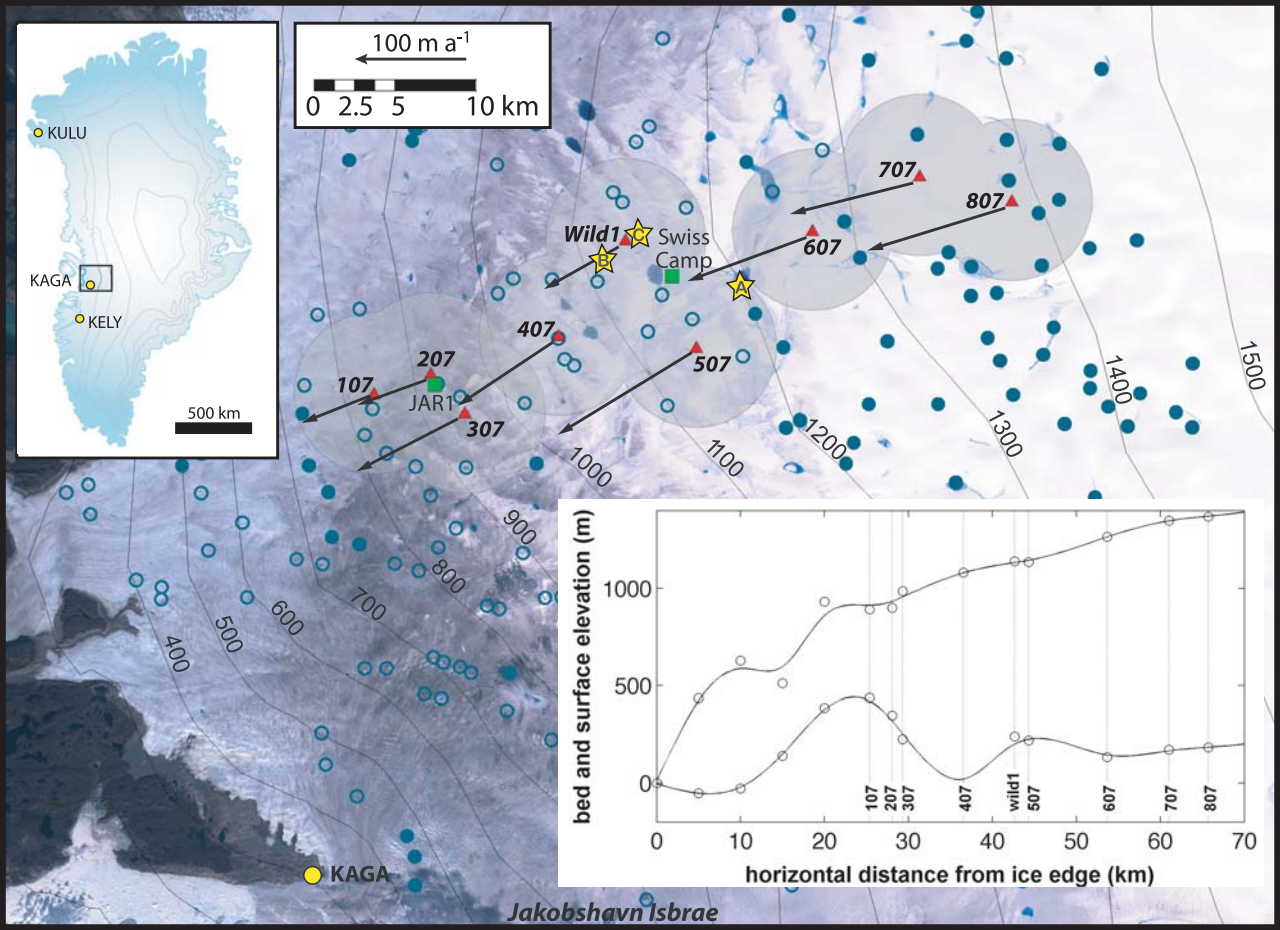
100 m a-1
0 2.5 5 10 km
KULU
KAGA
KELY
500 km
Wild1
Swiss Camp
JAR1
107
207
307
407
507
607
707
807
400
500
600
700
800
900
1000
1100
1200
1300
1400
1500
KAGA
Jakobshavn Isbrae
bed and surface elevation (m)
horizontal distance from ice edge (km)
0
500
1000
0 10 20 30 40 50 60 70
107 207 307 407 wild1 507 607 707 807

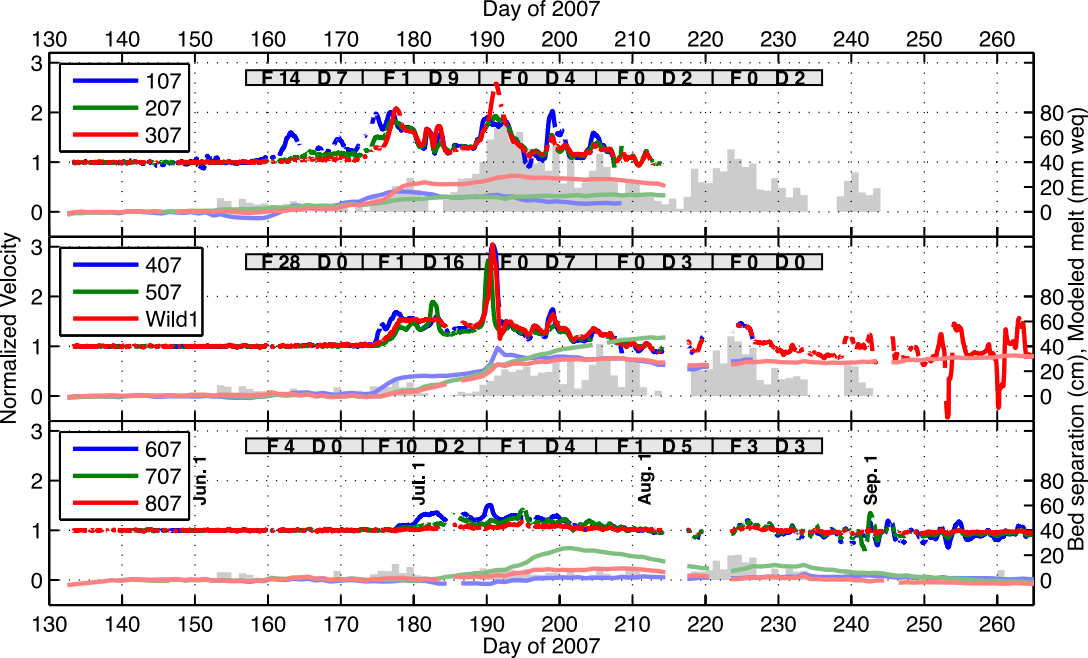
Day of 2007
Normalized Velocity
Bed separation (cm), Modeled melt (mm weq)
107
207
307
F 14 D 7
F 1 D 9
F 0 D 4
F 0 D 2
F 0 D 2
407
507
Wild1
F 28 D 0
F 1 D 16
F 0 D 7
F 0 D 3
F 0 D 0
607
707
807
F 4 D 0
F 10 D 2
F 1 D 4
F 1 D 5
F 3 D 3
Jun. 1
Jul. 1
Aug. 1
Sep. 1

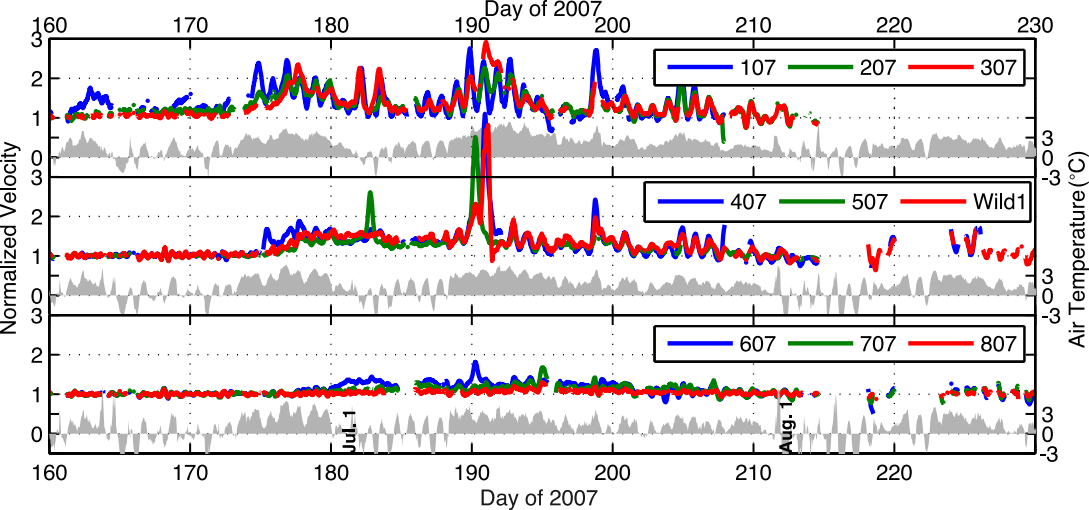
Day of 2007
160
170
180
190
200
210
220
230
Normalized Velocity
Air Temperature (°C)
107
207
307
407
507
Wild1
607
707
807
Jul. 1
Aug. 1
Day of 2007

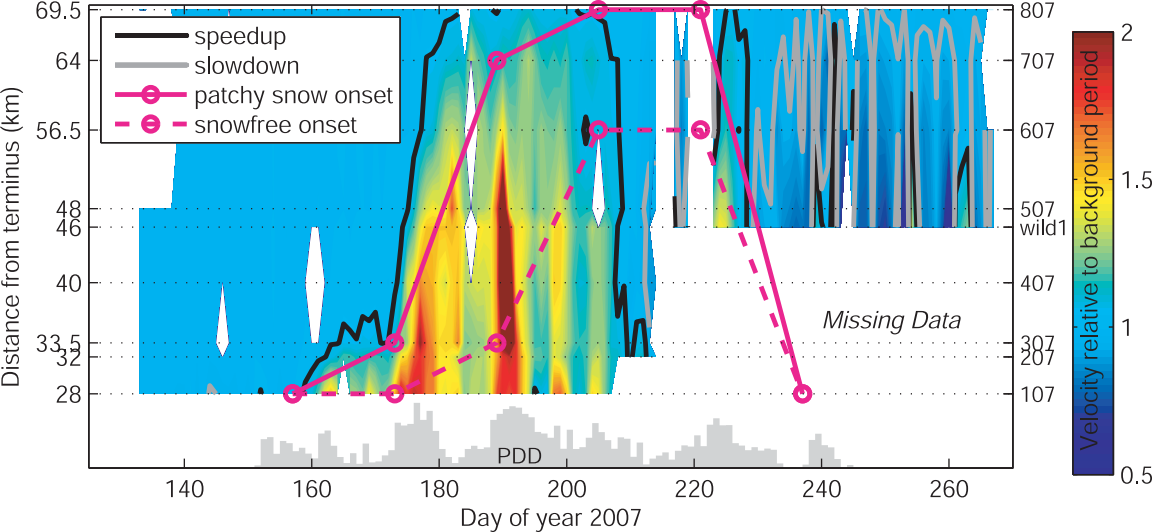
speedup
slowdown
patchy snow onset
snowfree onset
Missing Data
PDD
Distance from terminus (km)
69.5
64
56.5
48
46
40
33.5
32
28
807
707
607
507
wild1
407
307
207
107
140
160
180
200
220
240
260
Day of year 2007
Velocity relative to background period
2
1.5
1
0.5

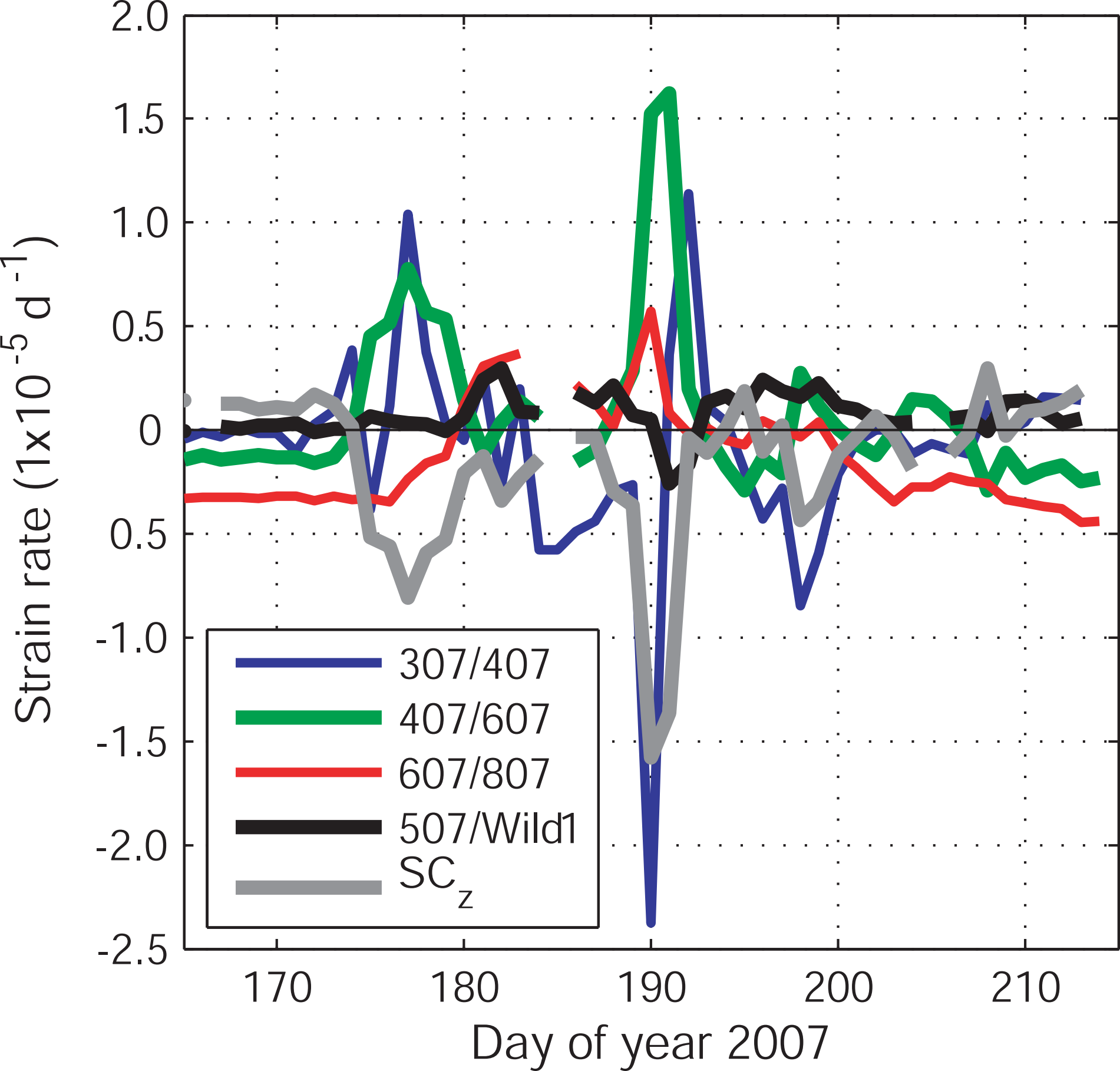
2.0
1.5
1.0
0.5
0
0.5
-1.0
-1.5
-2.0
-2.5
Strain rate (1x10^{-5} d^{-1})
170
180
190
200
210
Day of year 2007
307/407
407/607
607/807
507/Wild1
SC$_z$

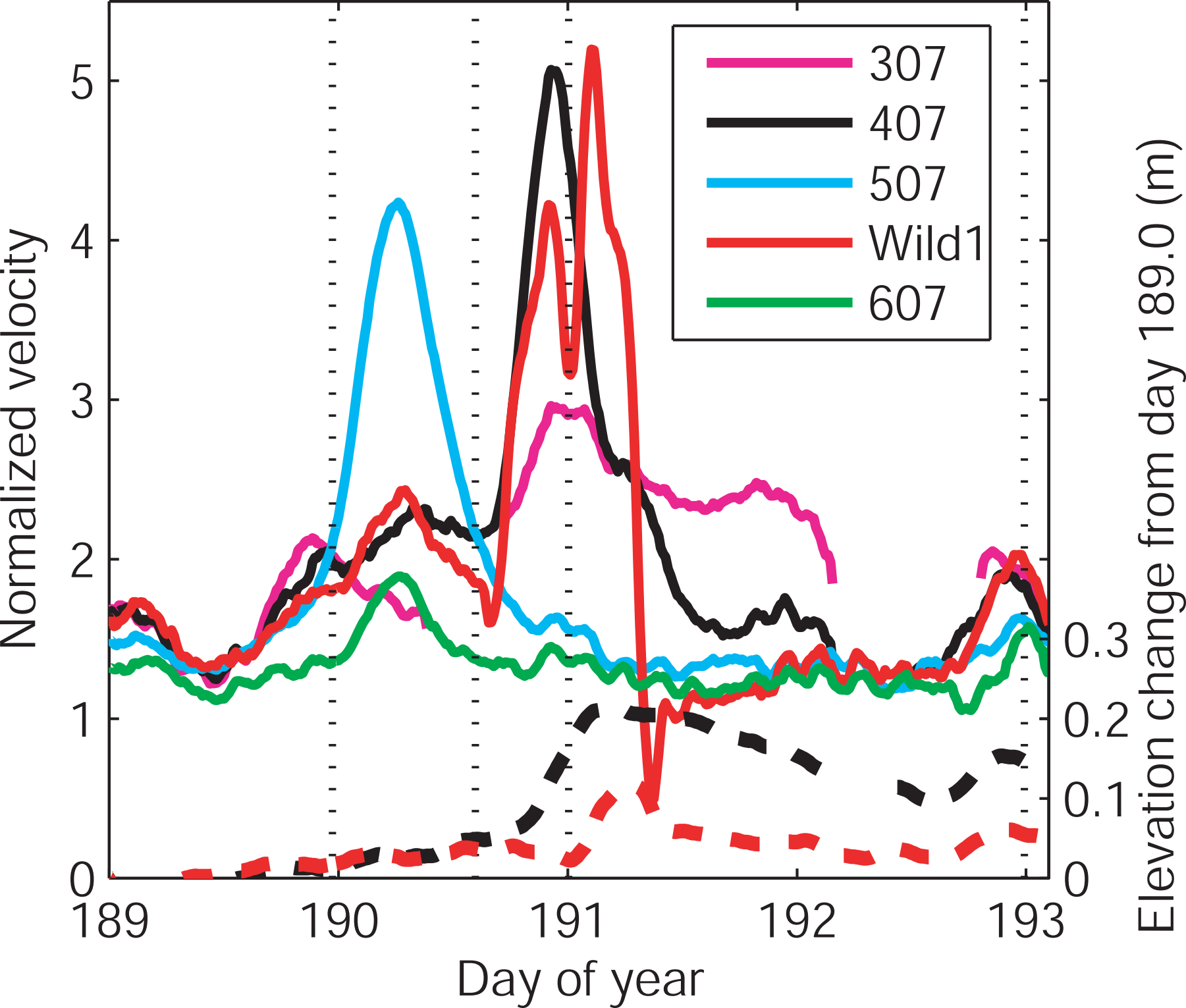
307
407
507
Wild1
607
Normalized velocity
Elevation change from day 189.0 (m)
Day of year
0
1
2
3
4
5
0
0.1
0.2
0.3
189
190
191
192
193

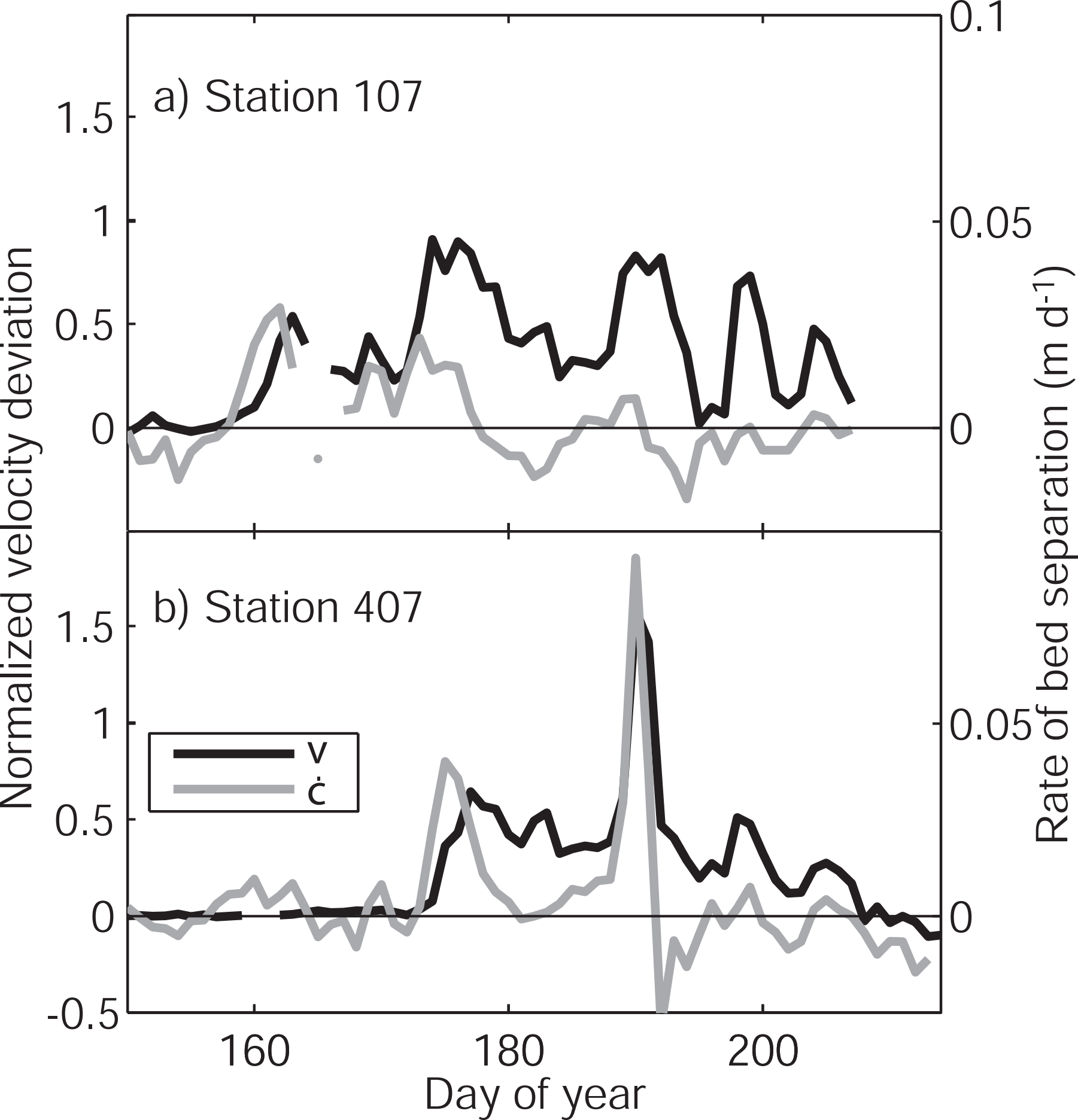
a) Station 107
b) Station 407
v
ċ
Normalized velocity deviation
Rate of bed separation (m d-1)
Day of year
1.5
1
0.5
0
-0.5
0.1
0.05
160
180
200

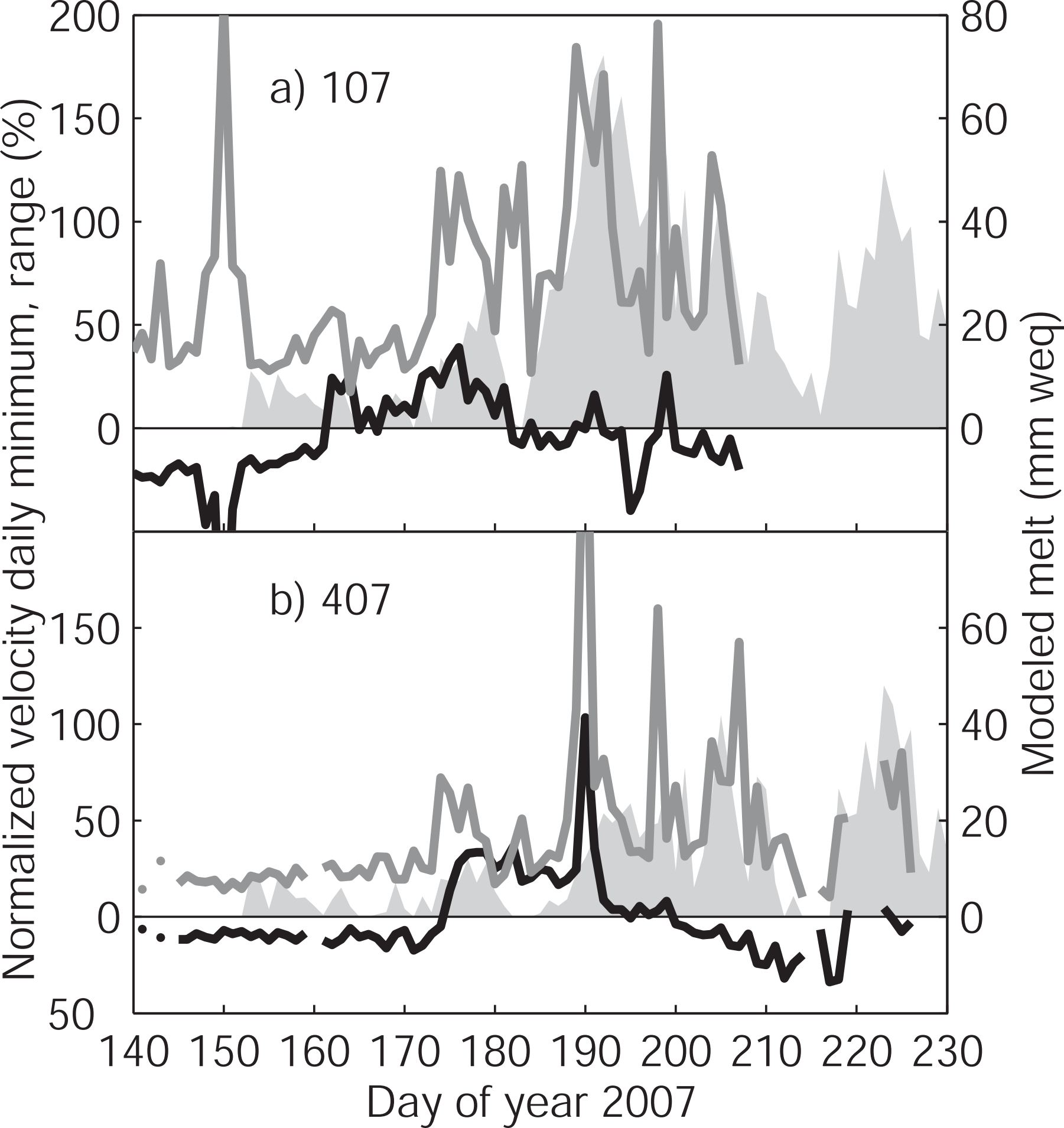
a) 107
b) 407
Normalized velocity daily minimum, range (%)
Modeled melt (mm weq)
Day of year 2007
200
150
100
50
0
80
60
40
20
0
150
100
50
0
50
60
40
20
0
140 150 160 170 180 190 200 210 220 230

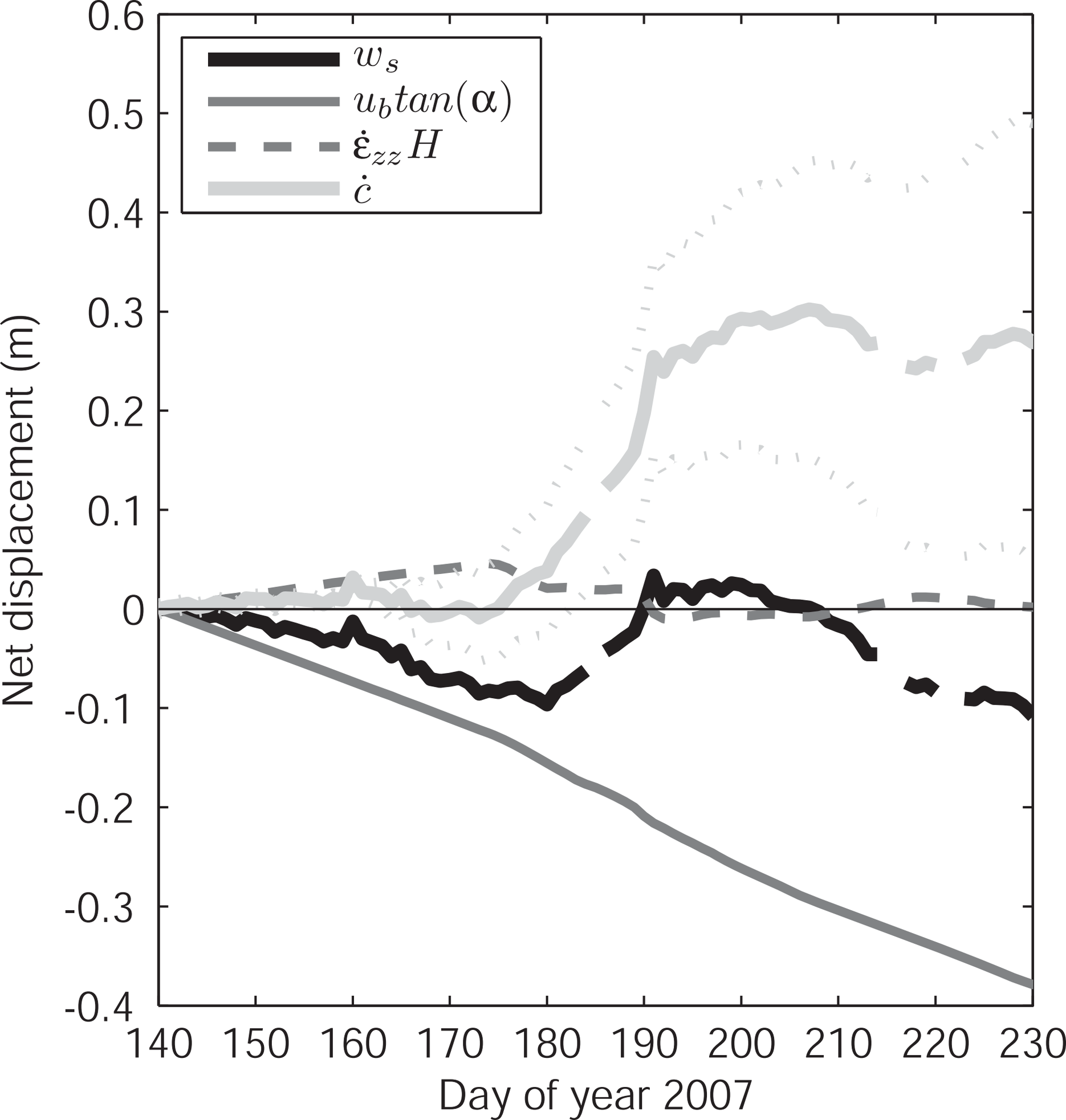
w_s
$u_b tan(\alpha)$
$\dot{\varepsilon}_{zz} H$
$\dot{c}$
0.6
0.5
0.4
0.3
0.2
0.1
0
-0.1
-0.2
-0.3
-0.4
Net displacement (m)
140
150
160
170
180
190
200
210
220
230
Day of year 2007